Materials Advances

ROYAL SOCIETY OF CHEMISTRY

REVIEW

View Article Online
View Journal | View Issue

Cite this: *Mater. Adv.*, 2022, 3, 756

Design of two-dimensional halide perovskite composites for optoelectronic applications and beyond

Tao Song, Qing-Xiu Ma, Qiang Wang * and Hao-Li Zhang *

Received 11th October 2021,
Accepted 19th November 2021

DOI: 10.1039/d1ma00944c

rsc.li/materials-advances

Two-dimensional (2D) halide perovskites have attracted increasing attention because of their unique optical and electronic properties, resulting in versatile applications in the fields of energy, information, display and lighting, *etc.* However, due to some unfavorable characteristics of 2D halide perovskites, such as their low carrier mobility and low radiation recombination efficiency, researchers have combined them with other functional materials to form composites with enhanced features not observed in their individual components, manifesting the positive "1 + 1 > 2" effect. In this review, we summarize the latest progress and future perspectives of 2D halide perovskite composites, focusing on their structures, fundamental optoelectronic properties, characterization techniques and typical use. 2D halide perovskite composites have become the most recently discovered goldmine to be exploited for endless possibilities beyond optoelectronic applications and require joint endeavors of researchers from interdisciplinary fields.

1. Introduction

Halide perovskites belong to the enormous perovskite family, which have the form ABX_3, where A is a monovalent cation such as methylammonium and alkali cation; B is a bivalent cation such as Pb^{2+}; and X is a monovalent anion such as a halide anion. The metal halide $[BX_6]^{4-}$ octahedral building blocks show great structural tunability in various formats including three-dimensional (3D), two-dimensional (2D), and one-dimensional (1D) or even zero-dimensional (0D) crystal structures.[1–3] In general, 2D perovskites can be divided into two types, where the first type includes traditional 2D geometric nanostructure morphologies such as like nanoplates and nanosheets, which are obtained by limiting the growth of their different crystal faces with an eventual thickness on the atomic scale.[4,5] The second type is electronically "2D" even in the bulk, with a crystallographic-stacking layered crystal structure. Note that both 2D perovskites and 3D perovskites with a 2D morphology are discussed in this review.

State Key Laboratory of Applied Organic Chemistry (SKLAOC), Key Laboratory of Nonferrous Metal Chemistry and Resources Utilization of Gansu Province, College of Chemistry and Chemical Engineering, Key Laboratory of Special Function Materials and Structure Design, Ministry of Education, Lanzhou University, Lanzhou, 730000, China. E-mail: qiangwang@lzu.edu.cn, haoli.zhang@lzu.edu.cn

Tao Song

Tao Song received his Master's Degree in Chemical Engineering from Northwest Normal University. He is currently pursuing his PhD Degree in Physical Chemistry in Lanzhou University under the supervision of Prof. Qiang Wang. His interest focuses on the optoelectronic properties of perovskite materials.

Qing-Xiu Ma

Qing-Xiu Ma is currently pursuing her Master's Degree in Physical Chemistry in Lanzhou University under the supervision of Prof. Qiang Wang. Her research interest focuses on conductive pastes for flexible electronic devices.

Generally, if cut along the (100), (110) and (111) crystallographic planes of the parent 3D perovskite structure, 2D halide perovskites are obtained, which results in three different orientations. Among them, the (100) oriented perovskites are most intensively studied[6] and can be further divided into three types of alternating cations in the interlayer (ACI),[6,7] Dion–Jacobson (DJ) phase,[8] and Ruddlesden–Popper (RP) phase[9,10] according to the capping cation type and relative position between the inorganic layers. Among them, the RP phase with the general chemical formula of $L_2A_{n-1}B_nX_{3n+1}$ (here L is a large cation and A is a small cation) is the most popular, where n represents the number of metal halide octahedral layers between the two L cation layers.[11,12] An infinite n number indicates a 3D perovskite and a finite n number suggests an ideal quantum well (QW). Thus, by adjusting the size of n, tailored band gaps and quantum confinement effects can be achieved.[13]

Moreover, with a hydrophobic organic spacer, 2D halide perovskites generally exhibit greater moisture resistance than their 3D counterparts. Due to their high photostability, chemical stability and tunable optoelectronic properties, 2D halide perovskite materials have found broad applications in fields such as solar cells and light-emitting diodes (LEDs) in recent years.[14,15] Usually in these devices, crystals growing along the vertical direction of the substrate in the film contain numerous phases instead of a single phase. The 3D phase generally has a smaller exciton binding energy and is more appropriate for application in solar cells. The 2D phase with a relatively high exciton binding energy is more appropriate for application in luminescent LEDs. Meanwhile, electrons and holes can transfer between different phases based on the energy level, with electron transport occurring from the 2D phase to 3D phase, whereas the reverse occurs for holes. Hence, depending on the type of device, the direction of crystal growth is crucial. Specifically, a deposition of the 3D phase on the bottom is beneficial for forward devices given that it is more conductive to charge collection and transfer, whereas deposition of the 2D phase on the bottom is more favorable for reverse devices.[16]

Compared with single semiconductor devices, those based on heterostructures can effectively manipulate the generation, reorganization and transmission of carriers. Due to the unfavorable characteristics of 2D halide perovskites, such as low carrier mobility and low radiation recombination efficiency,[17] researchers have combined them with other optoelectronic materials to solve these shortcomings. In comparison with pristine perovskites, heterostructures consist of two or more materials with different energy levels and demonstrate enhanced performances not exhibited by a single material system. Due to the weak van der Waals coupling between the organic layer and the inorganic layer, the 2D perovskite sheets can be mechanically stripped from their bulk crystals. In particular, the possibility of the delamination of 2D perovskites allow them to form different van der Waals heterostructures with

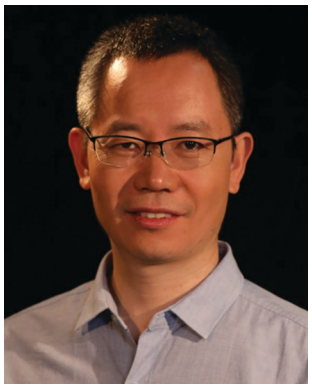

Qiang Wang

Qiang Wang received his BS Degree from Wuhan University in 1999. He then joined Prof. Yi Chen's group at the Institute of Chemistry, Chinese Academy of Sciences as a Graduate Student and performed research in the field of capillary electrophoresis (CE) and spectroscopic analysis. He obtained his MS Degree in 2002. Subsequently, he pursued his PhD Degree in Prof. Rosina Georgiadis' group at Boston University in the USA, developing novel label-free detection methods based on surface plasmon resonance (SPR). He transferred to Boston College in 2004 and worked on ultrafast time-resolved spectroscopy under the guidance of Prof. Torsten Fiebig. His main topics were focused on DNA photonics study on the femtosecond time scale and photoinduced electron and energy transfer processes in DNA upon photon excitation. He obtained his PhD Degree in May 2008 and became an Associate Professor of Chemistry at Lanzhou University in October. He was promoted as a Full Professor in 2017. His current research interests include nonlinear optics and ultrafast spectroscopy.

Hao-Li Zhang

Hao-Li Zhang received his BS in Organic Chemistry in 1994, and PhD Degree in 1999 from Lanzhou University. He then worked in the University of Leeds and Oxford University as a postdoc. In 2004, he was appointed as a Full Professor by the State Key Laboratory of Applied Organic Chemistry (SKLAOC) of Lanzhou University. He is currently the Deputy Director of SKLAOC and Deputy Dean of the College of Chemistry and Chemical Engineering. In 2014, he became a Fellow of The Royal Society of Chemistry (FRSC). He is an Editorial Board Member of Acta Physico-Chimica Sinica and Chinese Chemical Letters, and an Advisory Board Member of Chem. Soc. Rev. Prof. Hao-Li Zhang is interested in developing new organic functional materials for electronic and optoelectronic applications. He has published more than 240 research papers in peer-reviewed international journals with over 5000 citations, and his H index is 37. His current research projects include the design and synthesis of organic semiconductors; novel light-emitting materials; nonlinear optical materials; molecular electronics; and novel organic/inorganic hybrid materials for advanced optoelectronics.

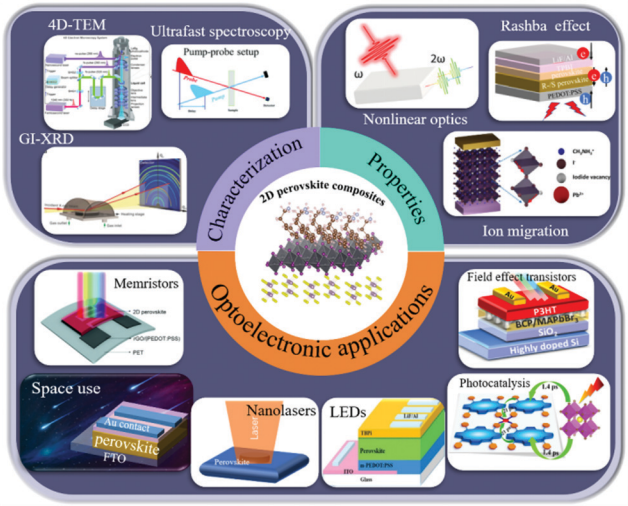

Fig. 1 Schematic illustration of 2D halide perovskite composite structures with versatile applications. Adapted with permission from ref. 18–25.

2D materials such as graphene, transition metal disulfides (TMDS), black phosphorus (BP) and other types of 2D perovskites.[26–28] These 2D/2D heterostructures have a sharp atomic interface without surface dangling bonds, which are especially important for high-performance and low-noise optoelectronic devices.[29] 2D perovskites can also be combined with 3D perovskites, organic polymers, carbon nanotubes (CNTs) and others to create optoelectronic devices with novel properties. Therefore, composite structures based on 2D halide perovskites will provide an excellent platform for the further exploration of new applications.

Our group have made contributions in this field by developing methods for the fabrication of novel perovskites and/or composites and studying their photoexcited state dynamics through various time-resolved spectroscopic techniques. In this review, we summarize the latest progress on composite structures based on 2D halide perovskites (Fig. 1), focusing on their structure, fundamental optoelectronic properties, characterization techniques and applications. Initially, we introduce the types and fabrication of 2D perovskite composites in Section 2. Subsequently, in Sections 3 and 4, the fundamental optoelectronic properties and common characterization techniques of 2D perovskite composites are discussed, respectively. We discuss these composites in detail based on their latest optoelectronic applications and beyond in Section 5. Finally, the prospects and challenges of this field are summarized in Section 6. This review is expected to provide new insights for the future direction of 2D perovskite composites.

2. Fabrication of 2D perovskite composites

2.1 General fabrication methods

The liquid phase method is the most commonly used method to prepare metal halide perovskites.[30,31] The growth process can be controlled by adjusting the surfactants in solution to obtain perovskite nanosheets directly, which are usually uniformly distributed and convenient for further processing. Many research groups have reported the synthesis of $MAPbBr_3$ and $CsPbBr_3$ nanosheets with a thickness of several nanometers in solution. Zeng *et al.*[32] prepared $CsPbBr_3$ nanosheets with a thickness of about 3.3 nm *via* a solution method for the first time using long-chain alkyl amine and oleic acid soft surfactant templates (Fig. 2a). Similarly, Manna *et al.*[33] obtained $CsPbBr_3$ nanosheets by introducing shorter alkylamines and longer oleic acid amines as ligands. The transverse size was adjusted by changing the ratio of shorter ligands to longer ligands, while the thickness was maintained at 3 nm (Fig. 2b). Liu *et al.*[34] synthesized $CsPbX_3$ nanosheets at a high temperature (170 °C) using long-chain carboxylic acids and short-chain amines as ligands. Dou *et al.*[35] directly grew large-area and atomic thin 2D halide perovskite sheets in solution (Fig. 2c), where ternary solvent mixtures were used and crystals grew during solvent evaporation. The atomic force microscopy (AFM) images confirmed that the thinnest sheet was a single-layer structure with a thickness of about 1.6 nm. This group[36] further used the liquid phase epitaxy growth method to inhibit the in-plane ion diffusion in 2D halide perovskites by rigid π-conjugated organic ligands, such as dithiophenylethylammonium (2T) and phenylethylammonium (PEA), to create a transverse heterostructure close to the atomic interface.

The substitution of organic ammonium ions for Cs^+ ions has been proven to be an effective method to transform perovskites into 2D RP layered structures and introduce quantum confinement effects. For example, Jie *et al.*[37] reported the colloidal synthesis of $(PEA)_2PbBr_4$ *via* the substitution of Cs^+ ion with PEA^+ (Fig. 2d). The large organic cations prevented water from

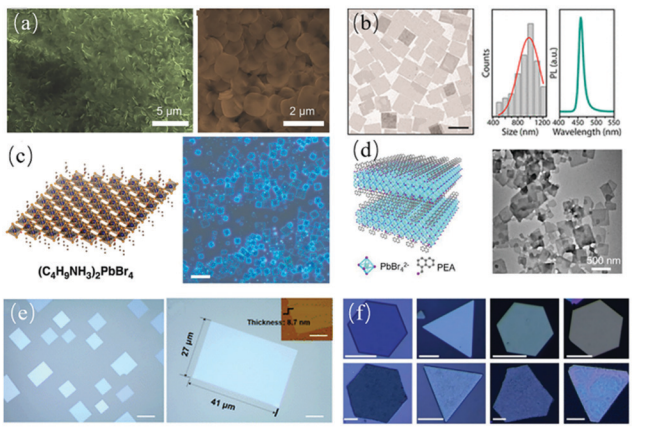

Fig. 2 (a) 2D $CsPbBr_3$ nanosheets. Low-magnification and high-magnification images. Adapted with permission from ref. 32. (b) TEM images of the $CsPbBr_3$ nanosheets (scale bar is 1 μm). Adapted with permission from ref. 33. (c) Structural illustration of a single layer of $(C_4H_9NH_3)_2PbBr_4$ and optical images of the 2D square sheets (scale bar is 10 μm). Adapted with permission from ref. 35. (d) Crystal structure of $(PEA)_2PbBr_4$ and TEM image of the 2D $(PEA)_2PbBr_4$ nanosheets. Adapted with permission from ref. 37. (e). Morphology of perovskite thin films (scale bar is 10 μm). Adapted with permission from ref. 40. (f) Optical microscopic images of 2D PbI_2 platelets (scale bar is 10 nm). Adapted with permission from ref. 41.

Table 1 2D perovskites synthesized *via* liquid-phase methods

Component	Temperature	Ligands	Atmosphere	Thickness	Preparation methods	Emission peak	Ref.
2D $CsPbBr_3$	140 °C	Oleyl amine (OAm), dodecylamine, and *n*-octylamine and oleic acid (OA)	N_2	3.3 nm	Hot-injection	—	32
2D $CsPbX_3$ (Cl^-, Br^- and I^-)	145–155 °C	Octanoic acid, octylamine, OA and OAm	N_2	3 nm	Hot-injection	452 nm	33
2D $CsPbBr_3$	140 °C	Hexanoic acid and OAm	N_2	2.6 ± 0.4 nm	Hot-injection	—	34
2D $(C_4H_9NH_3)_2PbBr_4$	75 °C	—	Ar_2	~1.6 nm (±0.2 nm)	Solvent evaporation	406 nm	35
$(2T)_2PbI_4$–$(2T)_2PbBr_4$	50 °C	Dithiophenylethyl-ammonium (2T)	N_2	5 nm	Solvent evaporation	520 nm	36
$(PEA)_2PbBr_4$	Room temperature	*n*-Octylamine	Air	4 nm	Anti-solvent recrystallization	410 nm	37
2D $(BA)_2(MA)_{n-1}$-Pb_nBr_{3n+1}	140 °C	—	Air	50–90 μm	Precursor acid precipitation	420–690 nm	48
2D $(PEA)_2PbBr_4$	Room temperature	Octylamine	Air	—	Anti-solvent recrystallization	415 nm	38

invading PbX^{4-} and improved the chemical stability. Zhao *et al.*[38] fabricated a 2D/3D perovskite composite by adding Cs^+ to 2D $(PEA)_2PbBr_4$ nanoplates, which combined the excellent stability of 2D perovskites and low exciton binding energy of 3D perovskites, showing promise for practical LEDs. Wright *et al.*[39] reported the preparation of a heterostructure of both horizontally and vertically aligned perovskite $(PEA)_2PbBr_4$ grown on 3D $CsPbBr_3$ in solution, which provided an ideal platform to study the physical properties and cross-heterojunction charge transfer process in more detail.[42] Table 1 summarizes the experimental conditions for the synthesis of 2D perovskites *via* liquid phase methods.

However, using the colloidal method, it is difficult to obtain larger sheets and mostly mixtures with different thicknesses are produced. In comparison, non-colloidal solution synthesis simply involves blending stoichiometric amounts of precursors to control the sheet thickness. Gas-phase growth, one of the commonly used methods for the synthesis of 2D materials, including chemical vapor deposition (CVD) and van der Waals epitaxy, is another popular method for the preparation of smooth large-area perovskite nanosheets. Xiong *et al.*[43] first used the van der Waals epitaxy method to grow lead halide nanosheets on mica, and then through the gas–solid heterogeneous reaction with methyl ammonium halide molecules, 2D perovskite nanosheets with a transverse size of 5–30 μm and thickness from several atoms to hundreds of nanometers were obtained. Subsequently, Shi *et al.*[40] reported the 2D van der Waals growth of 3D materials (non-layered semiconductors of $MAPbCl_3$) on ultra-thin mica (Fig. 2e). Although high-quality perovskites were obtained by this method, a substrate with a high melting point (>350 °C) was required during high-temperature growth, which is not suitable for flexible substrates with low melting points. Therefore, alternative methods need to be developed to produce 2D perovskites on different substrates, especially on flexible ones. To solve this problem, Li *et al.*[41] reported the controlled synthesis of 2D perovskite (Fig. 2f) on arbitrary substrates, including SiO_2/Si, Si, mica, glass and flexible polydimethylsiloxane (PDMS) substrates (as long as the melting point of the substrate was higher than 100 °C). The results showed that the gas-phase synthesis provided additional flexibility for the fabrication of a new 2D halogen perovskite composite.

2.2 Inorganic material/2D perovskite composites

Composite materials have played an indispensable role in the long history of materials development and use. After two or more components are combined in a specific order, the complex often exhibits the unique advantages of each component, thus improving the overall properties of the material. 2D perovskites have shown great potential as new materials for next-generation optoelectronic technology. Moreover, they can be synthesized at a low cost, providing more possibilities for their industrialization. However, the application of 2D perovskite is still limited by some inherent drawbacks such as low carrier mobility and low radiation recombination efficiency.[44] Accordingly, many researchers have combined 2D perovskites with inorganic materials to overcome these issues. In this section, we discuss the composite structure of 2D perovskite and inorganic materials based on the early and ongoing research progress.

The past few years have witnessed the rapid development of 2D van der Waals materials with unique physical and chemical properties. As one of the earliest 2D materials, graphene has shown extraordinary electronic, thermal and mechanical properties.[45] It is usually used as a carrier transport layer in heterostructures to obtain a greater gain. The heterostructure formed by the combination of 2D perovskite with graphene and its analogues has great potential in optoelectronic research. For example, Peng *et al.*[46] constructed photodetectors based on 2D perovskite $(C_4H_9NH_3)_2PbBr_4$ and monolayer graphene heterostructures (Fig. 3a) to enhance the performance of the devices. The covered monolayer graphene can protect the 2D perovskite crystals from dissolving in water or acetone, further increasing the device stability. TMDs are also used to construct heterostructures with 2D perovskites, usually forming II-type heterostructures. Duan *et al.*[47] reported a combination of perovskite

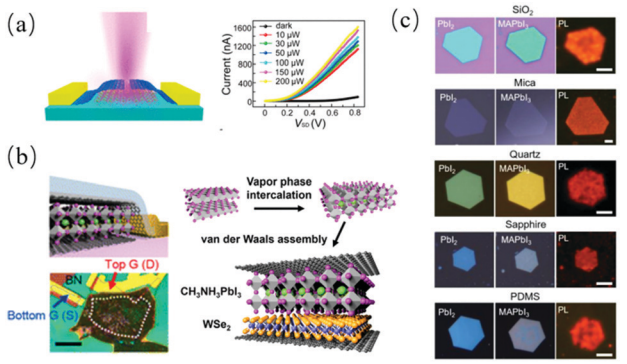

Fig. 3 (a) Schematic illustration of graphene-contacted 2D perovskite photodetector and current–voltage (I_{SD}–V_{SD}) curves. Adapted with permission from ref. 46. (b) Schematic diagram of the device structure. Adapted with permission from ref. 47. (c) Optical images of PbI_2 nanosheets, optical images and fluorescence photographs of $MAPbI_3$ nanosheets (scale bar is 5 μm). Adapted with permission from ref. 49.

and 2D materials through a layer-by-layer van der Waals assembly process to achieve a high photoconductivity gain of up to 2200 and high optical responsiveness of 950 A W^{-1} in a vertical heterojunction device (Fig. 3b). Through the effective protection of perovskite by boron nitride (BN), the lifetime of the perovskite 2D heterostructure was extended to 7 months. Li *et al.*[29] constructed photodetectors based on few-layer MoS_2 (n-type) and 2D perovskite $(PEA)_2SnI_4$ (p-type) heterostructures, which exhibited an amazing responsivity of 1100 A W^{-1} and high rectifier ratio of 500 under a bias of 3 V. Also, the heterojunction device could sense light in the whole range of visible and near-infrared wavelengths with an adjustable light response peak.

Andrew *et al.*[50] constructed a type II heterostructure of WS_2 monolayer/2D $(C_6H_5C_2H_4NH_3)_2PbI_4$ (PEPI) perovskite, which had a photoresponsivity 5-times higher than that of the WS_2 monolayer. Huang *et al.*[49] reported a reversible cation exchange of hybrid perovskite and effective surface functionalization of low-dimensional materials, showing the phase and heterojunction engineering of ultra-thin perovskites. Using PbI_2 as a precursor and template, perovskite nanosheets with different thicknesses and hexagonal shapes could be obtained on different substrates such as PbI_2, $MAPbI_3$ and $FAPbI_3$ (Fig. 3c). The transverse heterojunction of perovskite and PbI_2 was derived from a patterned single perovskite nanosheet using a mask made of a 2D material such as graphene, hexagonal boron nitride (h-BN) or MoS_2 to cover the template prior to the conversion of PbI_2 to perovskite. Perovskite-based vertical heterostructures were constructed through monolayer MoS_2 and $MAPbI_3$ stacking. The flexible design of perovskites and their integration with a variety of 2D materials offer numerous possibilities for new features and functions.

2D perovskites can also be compounded with other inorganic materials. Ren *et al.*[51] made a field-effect transistor (FET) using CNTs and the 2D perovskite $(PEA)_2PbI_4$ and achieved light-enhanced ion migration by changing the doping amount of CNTs. Meanwhile, the FET could achieve multi-stage optical memory by changing the excitation intensity. Ion doping was also used to regulate the optical, electrical and magnetic properties of 2D perovskites. Fu *et al.*[52] reported Mn^{2+}-alloyed 2D perovskite QW of Mn:$(PEA)_2PbBr_4$ (PEA, phenylethylammonium) with a high energy transfer efficiency (Φ_{ET} = 56%) and solid-state photoluminescence quantum yield (PLQY = 54%). Considering the huge tunability of 2D perovskites and large number of available inorganic materials, we expect that there is a lot of room for the exploration of composite structures with novel physical properties and expanded functions.

2.3 Organic material/2D perovskite composites

The selection of 2D perovskite composite materials is not only limited to inorganic materials. Organic materials have also been widely used to couple with 2D perovskites.[53] Compared with inorganic materials, organic materials can make use of their own hydrophobic interaction to reduce the contact between perovskite nanocrystals and the external environment, and thus increase the stability of the perovskite. Perovskites can also be modified by functional organic molecules (such as strong electron donor or acceptor) to contribute directly to the electron band, and thus promote charge separation.[54] Chemical modification in the form of chemical bonding is unique for organic material/2D perovskite composites and provides endless functionalization possibility for 2D perovskites.

Thus far, a large number of optoelectronic devices based on 2D perovskites have been constructed, and the stability of perovskites is the key to their practical application. Although several methods that encapsulated perovskites in a bulk matrix (for example, alumina[55] and silica[56]) improved the stability, the systems were usually complex macroscopic mixed materials, rather than nanostructures with clearly defined colloid dispersibility and processability. Through a dual protection layer, *i.e.*, an inorganic shell ligated with hydrophobic polymers, Lin *et al.*[57] developed an amphiphilic diblock copolymer method to prepare highly stable anisotropic $CsPbBr_3$ nanosheets (Fig. 4a). Anchoring other multi-dentate amphiphilic polymer ligands on the surface and templated growth of shell materials can create a rich variety of multi-functional and stable perovskite nanosheets.

In some recent studies, functional organic cations were introduced into 2D perovskites to change their photovoltaic properties. Samuel *et al.*[58] chose n = 1 layered perovskite with the molecular formula of (aromatic-*O*-linker-NH_3)$_2PbI_4$; naphthalene, pyrene, or perylenes as the aromatic moiety; and ethyl, propyl, or butyl as the linker. Through this method, customized synthetic organic cations were employed to enhance the out-of-plane conductivity of 2D perovskites (Fig. 4b).

Although the photovoltaic performance of materials can be significantly improved by using conjugated organic molecules as cations in 2D layered perovskite, the available organic cations of 2D layered perovskite are still limited because of their large volume.[59] Thus, to overcome this limitation, Dirk *et al.*[60] introduced charge transfer complexes into a 2D layered perovskite *via* self-assembly using pyrene-butylammonium (pyrene-C_4H_8-NH_3^+; $PyrC_4$) as the donor molecule, tetracyanoquinodimethane (TCNQ)

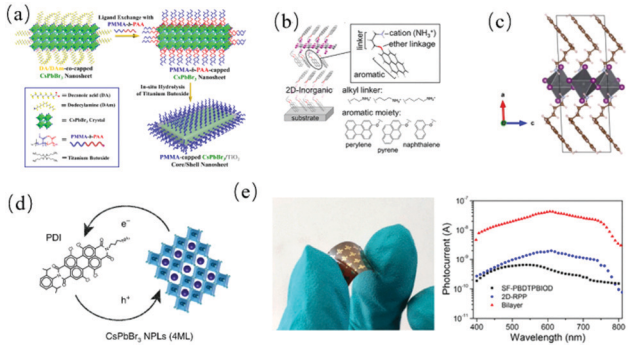

Fig. 4 (a) Schematic illustration of the fabrication of the $CsPbBr_3/TiO_2$ core/shell structure. Adapted with permission from ref. 57. (b) Layered perovskite and ammonium cation-linking method. Adapted with permission from ref. 58. (c) Unit cell of the $(PyrC_4)_2PbI_4$ 2D layered hybrid perovskite. Adapted with permission from ref. 60. (d) Schematic representation of the charge transfer between $CsPbBr_3$ NPLs and PDI molecules. Adapted with permission from ref. 54. (e) Flexible device and spectral photocurrents. Adapted with permission from ref. 62.

and tetracyanobenzene (TCNB) as strong acceptor molecules (Fig. 4c). Besides inducing charge separation, the strategy also opened up many other possibilities such as the use of chiral molecules or singlet fission/up-conversion chromophores. Ferdinand *et al.*[61] achieved charge separation by replacing non-conductive organic cations with organic charge-transfer complexes consisting of the electron-donor pyrene-alkylammonium (pyrene-C_n) and strong electron acceptor TCNQ. The microwave conductivity and femtosecond transient absorption showed that the light excitation of these charge transfer states led to long-lived moving charges in the inorganic layer, evidencing that charge separation could be induced in solid 2D perovskite by designing the organic layers. Recently, the same research group[54] went one step further to replace the non-functional organic ligands (Fig. 4d) on the surface of colloidal nanoplatelets with perylene diimides (PDI) to achieve the effective formation of mobile free charge carriers, which were generated at ten times higher yield with lifetimes (tens of microseconds) two orders of magnitude longer. The composites greatly enhanced the performance of the 2D perovskites.

Organic material/2D perovskite composites also show great potential in flexible optoelectronics. Wang *et al.*[62] designed a transverse photodetector by depositing a double-cable conjugated polymer SF-PBDTPBIOD (based on benzodithiophene (BDT) backbone polymer and perylene bisimide (PBI) side units) layer on 2D perovskite $(BA)_2(MA)_{n-1}Pb_nI_{3n+1}$ films (Fig. 4e). Due to the enhanced charge transfer and collection, the device exhibited a high responsivity of 27.06 A W^{-1} and an on/off ratio of 1379. The performance of the flexible device using polyimide as the substrate was comparable to that of the device on glass.

3. Optoelectronic properties of 2D perovskite composites

Metal halide perovskites have great advantages in optical and optoelectronic properties, such as high quantum yield,[63] high color purity,[64] adjustable band gap,[65] and high optical absorption coefficient.[66] Hybrid 2D halide perovskites perform even better in some aspects. For instance, 2D perovskite thin films with low defect density and good crystallization quality have high electron and hole mobility and transport equilibrium. Compared with the traditional III–V and II–VI materials, with a decrease in their size, the Coulomb force between electrons and holes in the 2D structure increases, and the dielectric constant between the organic layer and the inorganic layer is quite different. Thus these electron–hole pairs have higher binding energy and higher photoluminescence efficiency. Specifically, the following attributes of 2D halide perovskites are particularly noteworthy.

3.1 Strong exciton binding energy

One of the most interesting optoelectronic properties of 2D materials is their large exciton binding energy due to the decrease in dielectric shielding and quantum confinement effect.[67] For example, the exciton binding energy of monolayer WS_2 is as high as 700 meV. A large number of studies have reported the large exciton binding energy of 2D halide perovskites.[68–70] For these materials, due to the huge energy difference and high contrast of dielectric constant between their inorganic and organic layers, the Coulomb interaction between photogenerated electrons and holes is very strong, resulting in a significant oscillator strength and very large exciton binding energy (E_B, usually hundreds of meV), and hence efficient radiative recombination and high PLQY.[71,72] Note that the exciton binding energy of 2D perovskites can be fine-tuned *via* small-molecule intercalation. Smith *et al.*[73] stabilized 2D perovskite by inserting I_2 molecules into the binding spacer, which led to a more polarized organic layer than the inorganic layer and reduced the dielectric limitation of excitons. Their electronic, optical and magnetic properties can be adjusted accordingly.[13]

3.2 Tunable band gap

The band gap is one of the most important parameters of semiconductors. Narrow band gap perovskite semiconductors are widely used in devices related to photon absorption or emission. The optical properties of 2D perovskites depend on their crystal composition, the thickness of the perovskite layer and the dielectric contrast between perovskites and organic spacer. For example, in 2D perovskite nanosheets with the molecular formula of ABX_3, the valence band depends on the p-orbital of halogen X and the s-orbital of the B ion, the conduction band depends on the p-orbital of the B ion, and the ion at the A site does not have any effect on the electron transition. Adjusting the ratio of the B-site ion to halogen atom can tailor the band gap of 2D perovskites. The band gap also depends on the composition of the perovskite layers. With a decrease in the number of perovskite layers, the band gap of perovskite increases gradually.[74,75]

3.3 Ion migration

For perovskite-based optoelectronics, ion migration accounts for many unique behaviors such as current–voltage hysteresis, low-frequency giant dielectric response, and switchable photovoltaic effect.[76] Among them, the reversible structural swell–shrink

effect can be employed to fabricate tunable photonic/optoelectronic devices such as ultrafast solid-state displays, semi-transparent smart glasses and artificial retina devices.[76,77] The ion migration in perovskite materials is also applied to memristors.[78] Huang *et al.*[79] fabricated a 2D organometal trihalide perovskite-based memristor. By adding a bias voltage, the p–i–n structure was converted to an n–i–p structure, realizing a gradual change in the device resistance. Compared with 3D perovskites, 2D perovskites are more popular in memristors because of their enhanced stability. Ren *et al.*[80] constructed a single-crystal perovskite memristor based on a 2D RP phase, which showed outstanding resistive memory with a program current one order of magnitude lower than that of conventional materials, *i.e.*, as low as 10 pA.

However, ion migration may cause perovskite aging and destroy the device stability. For instance, ion diffusion often corrodes the charge transfer layer or metal electrode[81,82] of the device to accelerate the degradation of perovskite-based optoelectronics. Recent studies showed that long-chain organic ligands in 2D layered perovskite formed a barrier to prevent ions from migrating out of the plane and greatly improved the stability of the devices.[83] Huang *et al.*[84] synthesized single-crystal RP-type $BA_2MA_2Pb_3I_{10}$ (n = 3) to suppress the formation of iodide vacancies (V_I) and methylammonium vacancy (V_{MA}), and therefore ion migration along the electric channel in 2D perovskites.

3.4 Rashba splitting due to strong spin–orbit coupling (SOC)

The Rashba effect of perovskites stems from the strong spin–orbit coupling (SOC) with structural inversion asymmetry, which essentially affects the carrier dynamics, and thus the luminescence and photovoltaic performance of materials.[13,85] Vardeny *et al.*[86] measured the giant Rashba splitting in 2D $(PEA)_2PbI_4$ using the picosecond transient photo modulation technique. The perovskite showed a Rashba parameter of (1.6 ± 0.1) eV Å and a large Rashba energy splitting of (40 ± 5) meV. Mohammed *et al.*[87] further used density functional theory (DFT) and time-resolved spectroscopy to study the Rashba effect of a series of organic–inorganic hybrid perovskites. They found that inherent Rashba splitting occurred in the perovskite crystals with an even number of inorganic layers (n = 2), proving that stable perovskites with a large Rashba effect could be designed by artificially controlling the number of layers. Recently, they reported 2D (3AMP)PbI_4 and (4AMP)PbI_4 (3AMP = 3-(aminomethyl)piperidinium; 4AMP = 4-(aminomethyl)piperidinium) in a DJ phase, the hot-carrier cooling kinetics of which could be controlled by Rashba band splitting.[88] These studies imply that 2D perovskites may result in new breakthroughs in the development of semiconductor spintronics. However, the influence of the Rashba effect on the lattice distortion and dynamics in 2D perovskites remains largely elusive.

4. Characterization techniques for 2D perovskite composites

Besides the conventional spectroscopic techniques including steady-state absorption and fluorescence spectroscopy, laser confocal scanning microscopy for the investigation of optical properties, transmission electron microscopy (TEM) and scanning electron microscopy (SEM) for the investigation of morphology, X-ray photoelectron spectroscopy (XPS) and X-rays diffraction (XRD) for the investigation of the structures of perovskites, one noteworthy trend is the application of many advanced characterization techniques, such as highly time and spatially resolved and *in situ* methods.

4.1 Highly time-resolved techniques of ultrafast spectroscopy

Femtosecond transient absorption spectroscopy has become one of the most powerful approaches to disentangle the complicated excited-state photo physics and photochemistry of optoelectronic materials. In our previous review,[22,89,90] we summarized the study of the excited-state dynamics of 2D materials by ultrafast spectroscopy. Many of the applications of perovskites are also closely related to their photoinduced dynamics, which is crucial for understanding the origin of the excellent optoelectronic features of materials.

In recent years, the in depth study on the ultrafast process of 2D perovskite materials has also been widely reported. Beard *et al.*[95] reported the phonon bottleneck effect in perovskites and the time scale of biexciton recombination by using transient spectroscopy. Sum *et al.*[96] reported the dynamic process of extracting hot electrons from perovskite materials. Feldmann *et al.*[91] used femtosecond differential transmission spectroscopy to compare the carrier relaxation and recombination kinetics in 2D and quasi-3D halide perovskites (Fig. 5a), and the hot electron relaxation process and transient absorption in 2D perovskites. The basic understanding of carrier dynamics in perovskite composites is very important for their applications in optoelectronic devices. Knowledge of these processes is critical to design optoelectronic devices that rely on fast relaxation and charge- or energy-transfer mechanisms. Our group synthesized $CsPbBr_3$ quantum dots (QDs) based on our previously developed mechanochemical methods.[97] A type I 3D $CsPbBr_3$/2D $CsPb_2Br_5$ heterojunction was constructed by introducing excess $PbBr_2$ to transform $CsPbBr_3$ into $CsPb_2Br_5$ *via* a

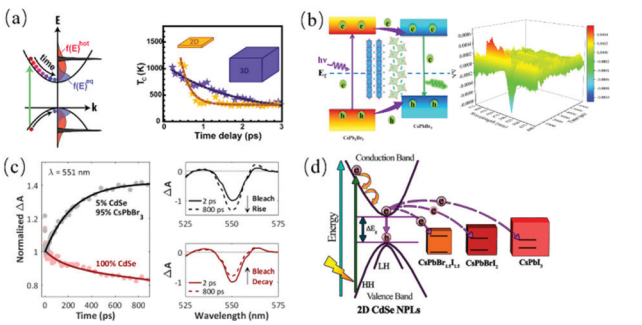

Fig. 5 (a) Thermalization and relaxation of photoexcited electrons and holes and transient carrier temperature cooling curves of quasi-3D and 2D perovskites. Adapted with permission from ref. 91. (b) Carrier dynamics of $CsPbBr_3$/$CsPb_2Br_5$ heterojunction nanosheets and 3D spectra. Adapted with permission from ref. 92. (c) Evidence for an influx of electrons into CdSe from $CsPbBr_3$ through transient absorption. Adapted with permission from ref. 93. (d) Photo-induced ultrafast electron transfer from CdSe to $CsPbX_3$. Adapted with permission from ref. 94.

phase transition (Fig. 5b).[92] Femtosecond transient absorption spectroscopy was employed to explore the carrier dynamics of the heterojunction, which provided the first observation of a $CsPb_2Br_5$ crystal signal in transient absorption spectra. The type I hierarchical structure enhanced the composite stability, prolonged the lifetime of photogenerated carriers, and resulted in a higher quantum yield. With the perovskite composites and additive phosphors, a white LED with a 94% color rendering index was obtained.

Richard *et al.*[93] reported the electron transfer between 0D and 2D nanoplatelets of $CsPbBr_3$ and CdSe. The electronic interactions among the 0D–0D, 0D–2D and 2D–2D systems were compared using static and transient absorption spectroscopy. The transient absorption measurement disclosed the ultrafast transfer of an influx of electrons into CdSe from $CsPbBr_3$ (Fig. 5c). Amitava *et al.*[94] reported the preparation of composites of 2D layered CdSe and $CsPbX_3$ perovskite nanocrystals. The kinetics of ultrafast electron transfer in the composites was studied by femtosecond spectroscopy (Fig. 5d). The sample was excited at low energy (<5 μJ cm^{-2}) at 400 nm to eliminate the multiexciton process. In the presence of $CsPbX_3$, the in-band relaxation of pure CdSe (800 fs) decreased sharply to <100 fs. Moreover, the ultrafast electron transfer from CdSe to the perovskite increased with an increase in the content of $CsPbX_3$ iodide composition (Fig. 5d).

4.2 High spatial resolution

The development of TEM techniques enables the internal structure of matter to be observed and characterized on the atomic and molecular scale. However, the instability of perovskites during electron beam irradiation results in a huge challenge to characterize their internal atomic/dynamic structures using conventional TEM techniques. In this context, various new techniques including cryoelectron microscopy (cryo-EM), spherical aberration correction TEM, and *in situ* TEM have emerged. Cryo-EM allows the observation of systems where traditional electron microscopy is powerless, such as biomolecules. Different from the traditional electron microscope using a charge coupled detector (CCD), cryo-EM uses a direct electron detector (DED), which has a better detection quantum efficiency and higher signal-to-noise ratio and can be used for imaging under lower electron radiation. Cui *et al.*[98] reported the structure and decomposition mechanism of perovskite materials in the environment by cryo-EM for the first time, where atomic resolution imaging of $MAPbI_3$ was illustrated (Fig. 6a). The iodide nanoparticles precipitated on the surface of $MAPbI_3$ after short-time UV irradiation and surface roughening after exposure to air for 10 s, a phenomenon never observed by XRD techniques. The authors established the definition of a critical electron dose, where that for $MAPbI_3$ at low temperature was 12 e^- $Å^{-2}$, and the spatial resolution was 1.49 Å. Similarly, the photostability of perovskite is a serious issue, but its mechanism remains controversial. It has been reported that the photoluminescence of $CH_3NH_3PbI_3$ thin films increases significantly under light, which is attributed to the photo-assisted migration of I^- ions.[99] Recently, Sui *et al.*[100] used quasi-*in situ* TEM for the first time to observe the

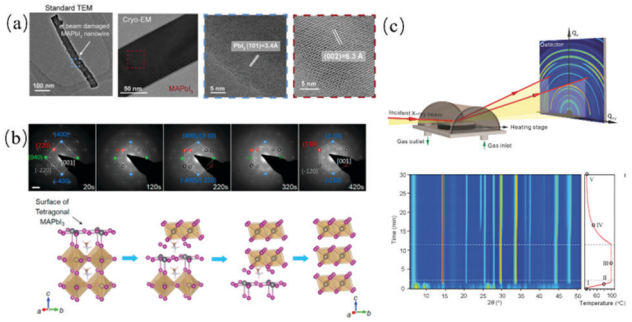

Fig. 6 (a) TEM images of $MAPbI_3$ nanowires with atomic resolution. Adapted with permission from ref. 98. (b) *In situ* structural evolution of $MAPbI_3$. Adapted with permission from ref. 104. (c) *In situ* GI-XRD measurements of the perovskite. Adapted with permission from ref. 21.

photodegradation of $MAPbI_3$ thin films at the grain boundary, accompanied by the formation of Pb^0 particles. The growth kinetics of the Pb^0 particles obeyed the exponential law of $r \propto t^{1/2}$, indicating that the degradation model was determined by the interfacial diffusion of elements. The quasi-*in situ* study indicated that the perovskite film degradation was accompanied not only by the production of Pb^0 but also the deposition of I_2. Thus, the use of advanced TEM techniques to understand the specific degradation mechanism of 2D perovskites provides useful insights for the development of more stable and effective optoelectronic devices.

Nuclear magnetic resonance spectroscopy (NMR), one indispensable tool for identifying organic molecular composition and structures, also finds applications to explore the large composition tunability and rich structural dynamics typical of 2D perovskites.[101] NMR as structural analysis technology is advantageous to detect the structure and dynamics of heavy and light elements, as well as the interaction between them through heteronuclear correlation experiments.[102] NMR is becoming increasingly beneficial to characterize and clarify the role of organic cations in 2D perovskites, which not only identifies the structure of the organic spacer layer and inorganic metal halide perovskite layer, but also determines the interactions between them. Especially for perovskites with a mixed organic spacer, which is difficult to characterize using diffraction techniques, NMR shows superiority. Vela *et al.*[103] first used ^{207}Pb solid-state NMR to monitor the degree of alloying and phase separation in mixed halide perovskites with the general formula of "$CH_3NH_3PbX_{3-a}X'_a$" (X, X′ = I, Br or Cl), revealing the existence of nonstoichiometric impurities or "dopants". Recently the sensitivity of ^{207}Pb has been significantly improved and the measurement time has been dramatically reduced by applying advanced NMR techniques such as magic-angle spinning (MAS), low temperatures, dynamic nuclear polarization (DNP), and proton detection.[105] Lee *et al.*[102] detected and quantified the composition and local structural characteristics of 2D RP phase $BA_2MA_{n-1}Pb$ by combining ^{207}Pb and 1H nuclear solid-state NMR. 1D NMR spectra were used to identify each Pb and H site. The ^{207}Pb–^{1}H 2D heteronuclear correlation (HETCOR) experiment disclosed the spatial proximity between them. Thus, by

determining the structure and dynamics of the organic and perovskite components in the RP phase, one can better understand the local atomic environment in the material.

4.3 Time- and space-resolved multidimensional techniques

Time- and space-resolved multidimensional techniques are powerful for investigating 2D perovskites. With the combination of microscopy and ultrafast laser sources, these techniques are especially suitable for the study of dynamic processes with high time and space resolution, among which time-resolved photoluminescence (TRPL) microscopy[106] and transient absorption (TA) microscopy[107] are representative ones.

Transient absorption microscopy combines the ultrafast spectroscopic method and optical microscopic technique to investigate material dynamics in both space and time. Moran *et al.*[108] imaged the electron excitation dynamics in the quantum well of the layered 2D perovskite $(PEA)_2(MA)_{n-1}[Pb_nI_{3n+1}]$ by transient absorption microscopy and compared the layered thin film with a pure phase single crystal to determine the diffusivity and two-body recombination rate. Recently, their team further combined linear spectroscopy with transient absorption microscopy to illustrate the mechanism of light-induced energy and charge transfer in layered perovskites. The specific carrier mobility trajectory[38] of the layered perovskite system could be determined by the cyclic laser pulse sequence and external bias applied to photovoltaic cells. These findings shed light on the rational design of 2D perovskite-based high-performance optoelectronic devices.[107]

Mohite *et al.*[106] studied the 2D layered perovskite $(BA)_2(MA)_{n-1}Pb_nI_{3n+1}$ with n from 1 to 5 by using confocal spatial photoluminescence (PL) mapping with a resolution of $\approx$1 μm. They found that the lower energy edge states dominated the photophysics of 2D layered perovskites with $n > 2$ by dissociating excitons into longer-lived free carriers. Jin *et al.*[109] developed a time-resolved photoluminescence imaging microscope with a sub-micrometer spatial resolution ($\approx$1 μm). They studied layered $(BA)_2(MA)_{n-1}Pb_nI_{3n+1}$ single crystals and discovered that the crystal edges with exciton dissociation ability were induced by the loss of BA ligands. Later, the same group observed long-distance carriers beyond the exciton limit in 2D perovskites.[110] Using confocal fixed-point excitation of a single crystal, the luminescence of the "boundary state" of the low energy state at a certain distance from the excitation point was observed. Given that there was no recombination luminescence on the carrier transport path, they speculated that the carriers travelled in a non-luminous "dark state" in the crystal and proposed a new mechanism of long-distance carrier transport assisted by defect states.

4.4 *In situ* techniques

In situ technology can track the changes in the structure, composition, morphology, and optoelectronic properties of perovskites in real time. The more commonly used techniques include *in situ* transmission TEM,[111] *in situ* XPS,[112,113] and *in situ* XRD.[21] *In situ* TEM is used to study the degradation process of perovskites to solve their instability problems, where the changes in their structure and morphology are observed in real time at the atomic level. However, the high-energy electron beam will cause serious damage to the target area, and hence it is necessary to carefully examine whether the perovskite decomposition is caused by electron beam-induced decomposition. Ducati *et al.*[111] introduced *in situ* TEM observation of perovskites for the first time, where the effect of the manufacturing route on the thermal degradation of perovskite materials was studied. Duan *et al.*[104] observed the thermal-induced degradation of $MAPbI_3$ *in situ* under controlled gas flow and showed that the crystal gradually evolved from tetragonal $MAPbI_3$ to triangular lead iodide with a fixed crystallographic direction (Fig. 6b). Sheng *et al.*[114] observed the degradation of perovskites by adding a bias voltage. Although *in situ* TEM characterization tools provide important information about the degradation mechanism of perovskites, due to the influence of electron beam irradiation, more advanced *in situ* scaffolds and robust samples are needed for more in-depth understanding.

Alternatively, X-ray-assisted characterization technology has been proven to be a powerful tool to study the crystal structure, chemical composition and morphology of perovskite materials. The *in situ* X-ray techniques commonly used in the field include XRD,[115] XPS,[116] and synchrotron radiation. These techniques can be employed to comprehensively evaluate the chemical, structural, phase and morphological changes in perovskites. Chen *et al.*[21] observed *in situ* the formation process of perovskite films using X-ray grazed incidence diffraction (GI-XRD) based on synchrotron radiation, disclosing the transformation process of the films in different solvent vapor atmospheres (Fig. 6c). By adjusting the preparation conditions of the thin films, a highly efficient perovskite solar cell was fabricated. Different characterization methods can be used to understand perovskites from different perspectives. Advanced *in situ* methods are specialized in revealing how water, oxygen, heat and light act on the surface of perovskites and cause physical and chemical changes.

5. Applications

2D perovskites can be conveniently tailored to the specific application needs of traditional research areas.[12] Among the many exciting properties of 2D perovskites, their excellent optoelectronic features, such as large absorption coefficient, high carrier mobility, and long diffusion length, make them suitable for applications beyond conventional ones. For example, they can be used for one-component white light emission of solid-state lighting equipment[117] and have shown strong optical nonlinearity. Herein, we summarize the latest research progress on 2D perovskite composites in optoelectronic applications and beyond.

5.1 LEDs

In the past few years, 2D metal halide perovskites have become a promising candidate for high-performance LEDs. Compared with 3D perovskites, 2D layered perovskites usually have a

larger exciton binding energy (hundreds of meV), which leads to the enhancement of radiation recombination and higher PLQY. The formation of cascade energy structures in 2D perovskite thin films with mixed n (layer thickness) can promote rapid and effective energy transfer from a lower n quantum well (QW) to a higher n QW (in sub-nanosecond), resulting in reduced exciton quenching and enhanced radiation recombination. Compared with 3D perovskites without hydrophobic molecules, the incorporation of hydrophobic organic ligands and the enhanced van der Waals interaction between organic molecules lead to a significant enhancement in environmental and thermal stability.[118] Similar to traditional semiconductors, the luminous efficiency of optically excited or electrically excited charge carriers in perovskite materials is controlled by the relative intensity of radiative and non-radiative processes. Since the first halogen perovskite LED was reported in 2014, the device external quantum efficiency (EQE) has increased from ~0.1%[119] to ~23%.[120] Although the perovskite family has good tolerance to electronic defects, the electroluminescence efficiency achieved thus far shows that suppressing non-radiative recombination under electrical excitation is still a challenge. Non-radiative recombination is also an important mechanism of voltage loss in photovoltaic solar cells. Thus, to enhance the radiation emission process in LEDs, one of the most successful strategies is to use low-dimensional structures. Sargent *et al.*[15] used mixed perovskites of $(PEA)_2MA_{n-1}Pb_nI_{3n+1}$ (n = 1–5 and 10) with different quantum sizes to fabricate LEDs with an ITO/TiO_2/quasi-2D layered perovskite/F8(poly(9,9′-dioctylfluorence))/MoO_3/Au structure. The dynamics investigations indicated that the multi-phased perovskites channelled energy across an inhomogeneous energy landscape and concentrated carriers on smaller bandgap emitters, facilitating more effective radiation recombination.[121] You *et al.*[24] proposed a new passivation strategy for the defects at the grain boundaries. By adding ethoxylated trimethylolpropane triacrylate (ETPTA) to the antisolvent, passivation was realized both on the surface and in the bulk (Fig. 7a). By restricting the formation of defects, the authors obtained an efficient green perovskite LED with a maximum EQE of 22.49%. Di *et al.*[122] constructed an LED emitting layer by combining quasi-2D and three-dimensional (2D/3D) perovskites and insulating polymer bulk. The photogenerated excitation migrated from quasi-2D to low-energy sites within 1 ps. The ultrafast migration ensured that any non-radiative traps with an energy higher than the final emitting species became negligible. Radiative bimolecular recombination emission in the 3D region effectively eliminated the non-radiative recombination path, resulting in an EQE of 20.1% and photoluminescence QE close to 100%. However, the high-efficiency LEDs based on perovskite are still limited to small devices, and serious performance degradation is always observed when producing large-area perovskite LEDs. Yuan *et al.*[123] proposed a low-barrier crystallization pathway by partially anchoring amphiphilic L-norvaline molecules to a $[PbBr_6]^{4-}$ inorganic plate to form a new mesophase with quasi-2D geometry, which overcame phase separation to obtain high-quality large-area thin films (Fig. 7b). The LEDs possessed an active area of 9.0 cm^2 and EQE of 16.4%.

In addition to efficiency, stability and lifetime are key factors determining the eventual commercial application of perovskite optoelectronic devices. Appropriate device packaging strategies can improve their resistance to water and oxygen. Other strategies have also been reported. Ye *et al.*[126] built a composite structure by embedding $CsPbBr_3$ nanosheets into a lattice-matched Cs_4PbBr_6 crystal matrix. This design led to the improvement of surface passivation, enhancement of radiation recombination and inhibition of agglomeration, resulting in a high PLQY for the solid perovskite. Gao *et al.*[124] used $MAPbBr_3$ nanoplatelets as the luminescent layer and poly(9-vinylcarbazole):2-(4-biphenylyl)-5-phenyl-1,3,4-oxadiazole (PVK:PBD) as the passivation luminescent layer. The addition of the PVK:PBD polymer removed pinholes in the perovskite luminescent layer and inhibited the non-radiative current loss, showing a high luminescence of 10 590 cd m^{-2} at 12 V (Fig. 7c). Qi *et al.*[125] used 18-crown-6 and poly(ethylene glycol) methyl ether acrylate (MPEG-MAA) as additives in perovskite films, which coordinated with Pb^{2+} and suppressed the self-aggregation of phenylbutylammonium bromide (PEABr). Consequently, the structure conversion from quasi-2D into nanocrystalline perovskite was prevented and a low defect density and high environmental stability were realized (Fig. 7d).

In short, 2D or quasi-2D layered perovskites have high brightness, wide band color tunability and excellent color purity. Combined with other desirable features such as facile solution processability and composition flexibility, these materials demonstrate potential to become mainstream emitters for LEDs.

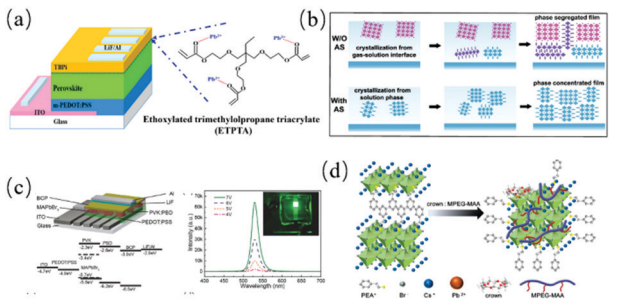

Fig. 7 (a) Device using ETPTA additive. Adapted with permission from ref. 24. (b) Growth of quasi-2D films without and with antisolvent. Adapted with permission from ref. 123. (c) Device architecture for a PeLED and electroluminescence spectra. Adapted with permission from ref. 124. (d) Defect passivation by crown and MPEG-MAA. Adapted with permission from ref. 125.

5.2 Solar cells

In recent years, the power conversion efficiency (PCE) of 3D perovskite solar cells has exceeded 25%,[127] which is comparable to that of crystalline silicon solar cells. However, the stability of perovskite solar cells seriously restricts their practical applications. Compared with 3D perovskites, their 2D counterparts offer an opportunity to overcome the stability issue because of the relatively higher chemical stability of the latter.[128] However, due to the existence of long-chain

complexes, the formation of multiple quantum well (MQW) structures in 2D perovskites limits the transport of photogenerated carriers, which usually reduces the photovoltaic performance.[129,130] In this case, the 2D/3D hybrid structure provides a balance by inheriting the good stability of 2D perovskites and the excellent photovoltaic performance of 3D perovskites. Indeed, perovskite solar cells based on these mixed structures show higher stability and improved PCE.[129] Snaith *et al.*[131] incorporated *n*-butylammonium cations into $FA_{0.83}Cs_{0.17}Pb(I_yBr_{1-y})_3$ 3D perovskites to form 2D perovskite sheets, which were scattered between highly oriented 3D perovskite grains and suppressed the recombination of non-radiative charge. An average PCE of 17.5% was obtained and the device remained stable in air for more than 1000 h. However, due to the existence of MQWs in 2D perovskites, the devices with 2D/3D mixed structures still need to sacrifice part of the efficiency of charge-carrier extraction. To solve this problem, Song *et al.*[129] inserted long-chain $EDBEPbI_4$ (EDBE = 2,2-(ethylenedioxy)bis(ethyl8bammonium)) into 3D perovskites to form a 2D/3D perovskite vertical heterostructure (Fig. 8a). The 3D perovskite grain boundaries were vertically passivated by 2D perovskites, which minimized the localization of photogenerated charge carriers in the low-dimensional perovskites. Also, the vertically arranged structure did not affect the charge carrier extraction from the 3D perovskites to the electrode, achieving a stable efficiency of 19.66%. The solar cells with an original efficiency of 90% were maintained after being placed in the air for three months (more than 3000 h). Dai *et al.*[132] introduced two hydrophobic short-chain alkyl ammonium salts (2-chloroethylamine, CEA^+ and 2-bromoethylamine, BEA^+) with halogen functional groups into $(Cs_{0.1}FA_{0.9})Pb(I_{0.9}Br_{0.1})_3$ 3D perovskites to obtain a 2D/3D perovskite structure (Fig. 8b). The cells exhibited a PCE of up to 20.08% under one sun exposure, and the initial efficiency of 92% was maintained after aging for 2400 h at 50% ± 5% relative humidity. Noh *et al.*[134] grew stable and highly crystalline 2D $(C_4H_9NH_3)_2PbI_4$ on 3D $(FAPbI_3)_{0.95}(MAPbBr_3)_{0.05}$ thin films to produce 2D/3D heterostructures. Given that the built-in potential was augmented at the 2D/3D heterojunction, a high photovoltage was obtained in the device. The heterojunction structure produced an open-circuit voltage of 1.185 V and PCE of 24.35%. Under the hygrothermal test (85 °C/85% relative humidity), the packaged device maintained 94% of its initial efficiency after 1056 h and 98% after 1620 h of full sunlight.

In addition, 2D perovskites can also be used in thermochromic smart windows. Sheng *et al.*[133] showed the robust and fast reversible thermochromic properties of 2D perovskite $(PDMA)(MA)_{n-1}PbnI_{3n+1}$ (PDMA = $C_6H_4(CH_2NH_3)_2^{2+}$ and MA = $CH_3NH_3^+$). After exposure to environmental conditions, the initial brown film became colorless upon the absorption of water, which was restored to its original color by heating at 100 °C for a few minutes or above 60 °C for several hours under ambient conditions (Fig. 8c). The reversible thermochromic property could be employed in applications such as thermochromic smart windows and thermochromic solar cells. For instance, as shown in the inset in Fig. 8d, the black box covered by perovskite windows reduced the indoor air temperature more effectively than that covered with pure glass in an enclosed space after 20 min-irradiation at 1.5 sun light intensity (~150 mW cm^{-2}). The photovoltaic devices with the $(PDMA)(MA{\cdot}H_2O)Pb_2I_7$ perovskite ($n = 2$) as the absorption layer displayed a PCE of more than 0.5% at high ambient temperatures.

5.3 Nanolasers

Low-dimensional perovskites have also shown huge potential in the lasing field, including edge-emitting amplified spontaneous emission (ASE), vertical-cavity surface-emitting lasers (VCSELs), miniature laser, and polaron laser.[135] Xiong *et al.*[136] demonstrated for the first time lasing based on the whispering-gallery-mode (WGM) optical resonant cavity with hexagonal and triangular shapes of $MAPbI_3$. Fu *et al.*[137] used the 2D perovskite $(BA)_2(MA)_{n-1}PbBr_{3n+1}$ to fabricate a WGM laser using a polydimethylsiloxane (PDMS) template. The ultrafast energy transfer together with the unique 2D perovskite quantum well (QW) structure concentrated the photogenerated carriers in the lowest-bandgap QW state. Consequently, the particle number inversion was easily established and spontaneous emission and laser amplification at room temperature were realized. The $\langle n \rangle = 6$ sample demonstrated an ASE threshold of 13.6 μJ cm^{-2} and a high gain coefficient (G) at least four-times that of 3D thin films (112 cm^{-1}). The results implied that 2D perovskites can be used for electrically driven lasers.

To enhance the stability of perovskites, Alex *et al.*[138] used $CsPbBr_3$ perovskite quantum dots and silica composite materials to fabricate WGM lasers. When immersed in water for 13 h, 80% of the initial emission quantum yield was maintained. Meanwhile, the thermal stability of perovskites is also very important for perovskite-based lasers. 2D materials, especially h-BN are widely regarded as ideal candidates for thermal management because of their high inherent thermal conductivity and high mechanical flexibility.[139,140] A recent report showed that the surface degradation of the $MAPbI_3$ microporous plate was inhibited and its thermal stability was greatly

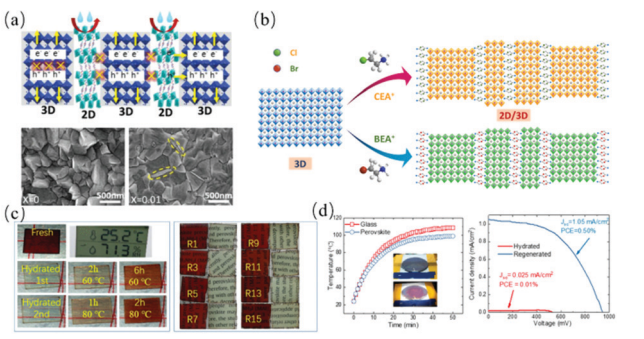

Fig. 8 (a) Schematic illustration of 2D–3D PVHH structure and SEM images of perovskite films with different 2D concentrations. Adapted with permission from ref. 129. (b) Self-assembled 2D/3D perovskite. Adapted with permission from ref. 132. (c) Prepared $(PDMA)MAPb_2I_7$ thin films. (d) Temperature changes with time and current–voltage curve of the solar cell with $(PDMA)MAPb_2I_7$ as the dynamic layer. Adapted with permission from ref. 133.

improved by using h-BN sheet packaging.[141] Dai *et al.*[142] synthesized $CsPbI_3$ nanosheets on muscovite substrates *via* CVD as gain materials and resonators to form high-quality WGM lasers. A covered perovskite–BN composite structure was prepared *via* the all-dry polydimethylsiloxane (PDMS) viscoelastic stamping method, which demonstrated excellent anisotropic thermal conductivity. Consequently, the heat dissipation of the perovskite nano-laser was accelerated and achieved clear laser behavior at a temperature of up to 75.6 °C. In addition, h-BN with high environmental stability can effectively protect perovskites from polar solvents. The $CsPbI_3$ nanolaser protected by h-BN lased continuously in water for 1 h, and the lasing behavior was maintained even after soaking in water for 24 h. The same group[143] further shielded $CsPbBr_3$ nanosheets from polar solvents *via* the atomic layer deposition (ALD) of Al_2O_3. After being coated by a thick Al_2O_3 layer of 50 nm, the $CsPbBr_3$ nanosheets emitted continuously in water for more than 1 h and still emitted after soaking in water for one month. Compared with the perovskite protected by h-BN, this method is simpler and more applicable to large-scale preparation.

Perovskite materials may also emit after two-photon absorption (TPA) or multiphoton absorption (MPA), and hence are promising candidates for up conversion lasers.[144,145] Perovskites with large TPA cross-sections are good optical gain materials. Zhao *et al.*[146] reported two-photon pumped lasers with linear and plate-like $MAPbBr_3$ microcrystals. Particularly, the unique QW structure of 2D perovskite helps to limit the electric charge carriers in the inorganic layer, thus enhancing the interaction between light and matter,[147] which is suitable for producing strong TPA.

5.4 Novel memory devices

In the context of the big data era brought by the Internet and cloud computing, traditional storage devices are required to demonstrate even higher memory performances including lower power consumption and faster data processing.[143] Halide perovskite has potential applications in resistance switchable memory because of its relatively low conductivity but good ion transport characteristics. However, currently, most halide perovskite resistive memory devices are based on 3D perovskite polycrystalline films, which usually contain defects on their surface and grain boundaries. Furthermore, due to their crystal structure transformation, chemical decomposition, and halide segregation, they are sensitive to oxygen and water and easily decompose. Ren *et al.*[148] studied the light-enhanced ion migration in perovskite single crystals by constructing a stripped 2D perovskite/CNT FET (Fig. 9a), where CNTs monitored the ion redistribution within the perovskite sheet upon photoexcitation. The device successfully displayed the optical and electrical multivalued two-phase photomemory effect.

Given that perovskites have a high light absorption efficiency, which is desirable for optical memory, recently, a new type of optical programming transistor memory was developed using a polymer-perovskite mixed dielectric layer, showing a good optical response, suitable on/off ratio and non-volatile

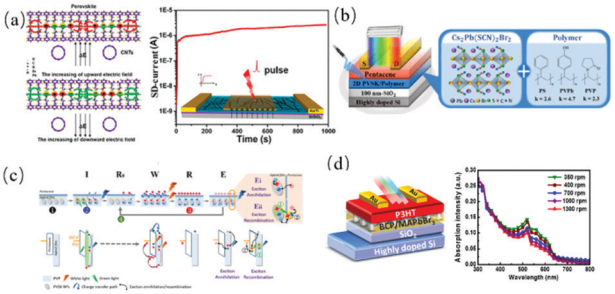

Fig. 9 (a) In-plane ion migration of perovskite under an electric field and photomemory test. Adapted with permission from ref. 148. (b) Device configuration of the studied photomemory and the structures of 2D $Cs_2Pb(SCN)_2Br_2$ and the host polymers. (c) Proposed operating mechanism of fully optically driven $Cs_2Pb(SCN)_2Br_2$/PVP-based photomemory. Adapted with permission from ref. 151. (d) Schematic image of the studied photonic synapse and optical absorption spectra of BCP/$MAPbBr_3$/P3HT prepared from different rotational speeds. Adapted with permission from ref. 23.

memory characteristics with long retention time.[149,150] Through space constraints, perovskite nanocrystals embedded in the polymer matrix may act as charge trapping sites to isolate charges, and the related trapping/untrapping mechanisms can be realized by applying an electric field or using photons. Chueh *et al.*[151] created a transistor memory through $Cs_2Pb(SCN)_2Br_2$/polymer (SCN^- = thiocyanide) hybrid films. The 2D $Cs_2Pb(SCN)_2Br_2$ with intrinsic QW structure exhibited not only a considerable photoresponse but also good environmental stability. In addition, three host polymers with different functional groups, including polystyrene (PS), poly(4-vinylphenol) (PVPh) and polyvinyl pyrrolidone (PVP) (Fig. 9b), were systematically studied for comparison. All the manufactured devices showed light-induced memory recovery behaviors. According to the preliminary analyses, the mechanism of the programming–reading–erasing–reading function was proposed (Fig. 9c). Chen *et al.*[23] constructed red-light-stimulated nonvolatile perovskite-based photomemory using $MAPbBr_3$/polystyrene-*block*-poly(ethyleneoxide) (BCP) as the charge trapping layer and poly(3-hexylthiophene-2,5-diyl) (P3HT) as the active channel. Through the energy level mismatch and isolation effect of the polymer matrix, the photogenerated holes in P3HT and perovskite were left in the P3HT layer, while the photogenerated electrons were stored in the perovskite (Fig. 9d). Benefiting from the synergistic effect between the two components, the optical memory based on P3HT/perovskite showed optically recordable behavior in the whole visible spectrum. The response under red light was optimized by manipulating the thickness of P3HT. Due to the limitation of the exciton diffusion length, the optimized thickness of P3HT was 7.54 ± 0.42 nm, the minimum characteristic time was 36.6 s and the maximum on/off current ratio was 3.62×10^5 under red light illumination (500 mW cm^{-2}).

5.5 Photodetectors

2D perovskites are promising candidates for optoelectronic detection due to their unique anisotropic charge carrier behaviors. Given that 2D perovskites composited with more materials can expand their functions, many fabrication strategies, such as

molecular beam epitaxy and metal–organic vapor phase epitaxy, have been employed to produce transverse and longitudinal heterostructures for photodetectors. Li *et al.*[152] prepared this type of heterostructure at low temperature through the combination of solution and gas–solid phase intercalation (Fig. 10a). However, this method only yielded polycrystals with relatively poor quality, and grains were introduced in the intercalation process, resulting in the poor performance of the photodetectors. Recently, Li's team[153] developed a solution method for the synthesis of highly stable $(C_4H_9NH_3)_2PbI_4/(C_4H_9NH_3)_2(CH_3NH_3)Pb_2I_7$ heterojunctions (Fig. 10b) with a centimeter size, high crystallization quality and narrow-band dual-frequency photoresponse. The photodetectors fabricated with this heterostructure exhibited a low dark current ($\sim 10^{-12}$ A), high on–off current ratio ($\sim 10^3$), narrow full-width at half-maximum (fwhm) (less than 40 nm) and efficient narrow dual-band spectra. Dou *et al.*[154] demonstrated a liquid-phase epitaxial growth method to improve the crystal quality of perovskite heterostructures. By inserting rigid π-conjugated organic spacers, such as dithiophenylethylammonium (2T), phenylethylammonium (PEA) and tetrathiophenylethylammonium (4Tm), the ion migration was significantly inhibited in the plane and led to atomically sharp heterostructures. Further simulations showed that conjugated ligands reduced the heterostructure disorder and increased the vacancy formation energy, thus forming a highly stable interface. Similarly, to overcome some disadvantages of 2D perovskites, such as instability, low carrier mobility and low radiation recombination efficiency,[155] researchers have combined 2D perovskites with other optoelectronic materials (such as graphene, TMDs, and BP) to construct van der Waals heterostructures. For example, Atwater *et al.*[162] prepared a heterostructure consisting of WS_2 and $(BA)_2(MA)_3P_4I_{13}$ hybrid perovskite (Fig. 10c) and observed improved stability and enhanced emission two orders of magnitude greater than that of WS_2. The first-principles calculation attributed the photoluminescence enhancement to the charge transfer between the interfaces originating from the dipole moment, which caused a local electric field and led to an indirect to direct band gap transition in the multilayer WS_2. Likewise, graphene can also form a heterostructure with 2D perovskites to stabilize them. Rand *et al.*[163] improved the stability of perovskite by covering a thin sheet of 2D $(PEA)_2PbI_4$ perovskite with a graphene layer to restrain the loss of iodide. An ultra-stable phototransistor based on the graphene/2D perovskite/graphene structure was demonstrated, which did not degrade for a period of 75 days (Fig. 10d).

The ultra-smooth surface and strong interface coupling of 2D perovskites provide an excellent platform for the design of new composite structures such as flexible materials and devices. Although progress has been made in perovskite-based flexible devices such as LEDs, photodetectors, solar cells and lasers,[164,165] studies on these devices with 2D perovskite composites are relatively rare. Recently Wang *et al.*[156] designed a transverse photodetector by stacking a double-cable conjugated polymer film on the top of the 2D perovskite $(BA)_2(MA)_3Pb_4I_{13}$, using polyimide as a flexible substrate. It displayed a high responsivity of 27.06 A W^{-1}, high on/off ratio of 1379, and rapid rise/fall time of 3.53/3.78 ms. Table 2 presents a summary of the performance of the recently reported photodetectors based on 2D perovskite composites. In general, the stability and operation duration of these flexible devices still need to be improved.

5.6 Nonlinear optical applications

Many of the above-mentioned perovskite nanolasers are based on the nonlinear optical properties of the materials. However, 2D perovskites also exhibit other types of nonlinear optics such as second harmonic generation (SHG) and third harmonic generation (THG). The study of nonlinear optics began with SHG, which was discovered by Franken in 1961.[166] With the development of high brightness and highly coherent laser sources, nonlinear optics has become one of the most important branches of optical research. Therefore, the study of nonlinear optical materials has fundamental scientific and technical significance.[167]

Studies have shown that large nonlinear optical responses are widely observed in many inorganic 2D materials, such as graphene oxide,[168] MoS_2,[169] hexagonal boron nitride (h-BN),[170] and BP.[171] Our research group also performed many studies on the nonlinear optics of 2D materials.[172–174] Different from ideal harmonic oscillators, a large number of thermally stable and delocalized excitons populate 2D perovskites and strongly interact. Consequently, 2D perovskites may exhibit strong THG under resonant excitation.[13] Abdelwahab *et al.*[175] mechanically exfoliated 2D perovskite nanosheets (Fig. 11a), which exhibited ultra-strong THG with a maximum effective third-order susceptibility ($\chi^{(3)}$) of 1.12 × 10^{-17} m^2 V^{-2} and maximum conversion efficiency of 0.006%.

For the specific centrosymmetric structure of 2D layered perovskites, it is difficult to produce a strong second-order nonlinear optical response. However, by incorporating 2D perovskites and organic materials (such as varying different ammonium functional groups), the structural symmetry can be adjusted. Xu *et al.*[176] used the chiral molecule of methylphenylethylamine (MPEA) as an organic component to induce the

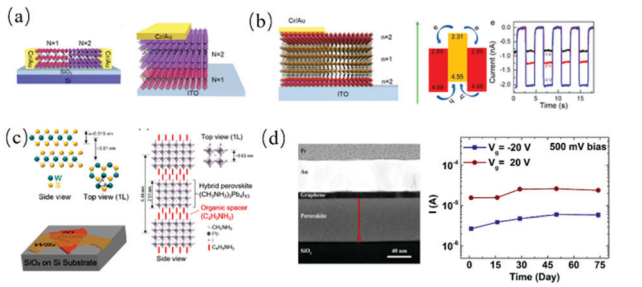

Fig. 10 (a) Electrical measurement and stability properties of as-grown lateral and vertical heterostructures. Adapted with permission from ref. 152. (b) Schematic illustration of the device configuration based on the $(BA)_2PbI_4/(BA)_2(MA)Pb_2I_7$ heterostructure. Adapted with permission from ref. 153. (c) Crystal structures and lattice constants of WS_2 and 2D perovskites (n = 4). Adapted with permission from ref. 162. (d) SEM image of the sandwich structure of graphene/2D perovskite/graphene and the photocurrent of the device stabilized for 75 days. Adapted with permission from ref. 163.

Table 2 Comparison of the performance the reported photodetectors based on 2D perovskite composites

Materials	Flexible base type	Photodetector architecture	Photoresponsivity (A W^{-1})	Detectivity (Jones)	ON/OFF ratio	τ_{rise}/τ_{fall} (ms)	EQE (%)	Operation wavelength	Ref.
$(PEA)_2SnI_42D/SnF_2$	Polyethylene terephthalate (PET)	rGO(reduced graphene oxide)/(PEDOT:PSS)	16	1.92×10^{11}	—	630/3600	—	470 nm	19
SF-PBDTPBIOD/$(BA)_2(MA)_3Pb_4I_{13}$	Polyimide (PI)	—	27.06	—	1379	3.53/3.78	—	White light	156
2D $CsPbBr_3$	PET/ITO	ITO/$CsPbBr_3$/ITO	0.64	—	$>10^4$	0.019/0.024	—	442 nm	32
$(iBA)_2(M_{1-x}FAx)_3Pb_4I_{13}$	Polyimide (PI)	—	0.4	1.68×10^{12}	720	43/22	—	532 nm	157
$(BA)_2(MA)_4Pb_4I_{13}$	PI	Au/$(BA)_2(MA)_3Pb_4I_{13}$/PI	0.17	3.7×10^{12}	2.3×10^3	24/65	—	750 nm	158
$CsPbBr_3$ nanosheets/CNTs	PET	Ag/$CsPbBr_3$ nanosheets/CNT/ITO/PET	31.1	—	90	0.016/0.38	7488	442 nm	159
$CsPbBr_3$ nanosheets/$Ti_3C_2T_x$	Paper	$CsPbBr_3$ nanosheet/$Ti_3C_2T_x$/paper	0.044	6.4×10^8	2.3×10^3	—	—	450 nm	160
$CsPbBr_3$	—	—	3.59	1.57×10^{12}	—	—	840	442 nm	161
2D $CsPbBr_3$/PCBM	PET	Au/$CsPbBr_3$/PCBM/ITO/PET	10.85	3.06×10^{13}	$>10^5$	0.04/0.39	3390	442 nm	161

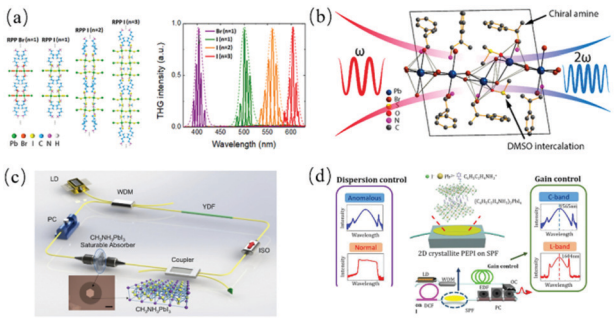

Fig. 11 (a) Structure of different 2D RPP crystals and the fundamental wavelength dependence of the THG spectra of the most effective flakes. Adapted with permission from ref. 175. (b) SHG of chiral perovskites. Adapted with permission from ref. 176. (c) Schematic diagram of the ring cavity of the mode-locked fiber laser. Adapted with permission from ref. 180. (d) Mode-locking using 2D $(C_6H_5C_2H_4NH_3)_2PbI_4$ saturable absorber. Adapted with permission from ref. 181.

non-centrosymmetric assembly of 2D inorganic layers (Fig. 11b). The 2D inorganic layers and perovskite crystals were assembled into a chiral *P*1 space group by anti-solvent vapor-assisted crystallization (AVC) with a structure of $(MPEA)_{1.5}PbBr_{3.5}(DMSO)_{0.5}$, where DMSO was dimethyl sulfoxide. Then novel 2D perovskite nanowires were grown by anti-solvent-assisted crystallization in the ternary solvent system, which showed a strong SHG response with high polarizability. Therefore, the introduction of different ammonium groups as organic spacers provides a general platform for the functionalization of 2D perovskites, giving them tunable nonlinear optical characteristics. SHG was also used to detect the interaction between photons and local structures of 2D perovskites. Lu *et al.*[177] found that the SHG intensity of 2D $[(C_6H_5CH_2NH_3)_2]PbCl_4$ depended on the thickness of the nanowires. DFT calculations and Monte Carlo (MC) simulations implied that the van der Waals interaction from flexible organic amine cations played a key role.[178]

The nonlinear saturable absorption of perovskite materials is of great use in mode-locked lasers. Perovskites can be inserted into the laser cavity by depositing on the end face of the optical fiber connector or the side polished surface of the D-shaped optical fiber for mode-locking.[179] Li *et al.*[180] used a single 2D $CH_3NH_3PbI_3$ nanosheet as the saturator for a 1064 nm ytterbium-doped fiber laser (Fig. 11c). Compared with the control films, the 2D perovskite nanosheets had stronger saturable absorption, larger modulation depth and lower saturable strength. In particular, the perovskite nanosheets with a thickness of 105 nm had the highest modulation depth of 22.2% and the lowest saturation strength of about 1.8×10^3 GW cm^{-2}. The fwhm of the stable mode-locked pulse output pulse was 931 ps, the signal-to-noise ratio was more than 53 dB, the peak power was 4.14 W, and the pulse energy was 3.85 nJ. Hong *et al.*[181] constructed an all-fiber ring laser cavity using a 2D perovskite microcrystalline film of $(C_6H_5C_2H_4NH_3)_2PbI_4$ as the saturated absorber and erbium-doped fiber as the optical gain medium (Fig. 11d) obtain transform-limited soliton pulses in the C and L bands under abnormal dispersion. The C-band soliton pulse showed a very short pulse duration of 381 fs and a spectral bandwidth of 7 nm with a central wavelength of 1565.9 nm and a high signal-to-noise ratio of more than 89 dB at a repetition rate of 41.88 MHz. Furthermore, L-band soliton pulses with a 6 nm spectral bandwidth were stably obtained at 1604 nm by adjusting the optical gain.

Lasers can impose great damage to optoelectronic devices and the human body (especially human eyes), and thus are also used as laser weapons. Laser protection has been a research frontier regardless of civilian or military use. Among them, optical limiters can reduce the transmittance of strong light and maintain weak light, well protecting the human eyes and precision optical sensors from damage caused by high-intensity light. Perovskite is a potential laser radiation-limiting material because of its two-photon and multiphoton absorption. Pai *et al.*[182] reported the optical confinement behavior of a lead benzylamine(II) perovskite bromide microdisk from strong TPA under 800 nm fs-laser excitation. A limiting offset of 1.2 mJ cm^{-2} was obtained, and the surmised optical limiting threshold of ~25.6 mJ cm^{-2} was comparable to that of benchmark materials such as 2D MoS_2.

Thomas *et al.*[183] also reported 2D RP organic–inorganic hybrid perovskite quantum dots with high optical confinement. Optical z-scanning experiments showed that the maximum optical limitation was 67% at 175 μJ under a 532 nm ns laser. The effective two-photon coefficient was 7.2×10^2 cm GW^{-1}.

Although 2D perovskites show remarkable nonlinear optical properties, especially their nonlinear absorption properties including saturated absorption and two-photon or multiphoton absorption, the stability of these materials remains the main obstacle for their practical applications. Accordingly, by compounding with different materials, such as adding organic functional cations, recombination with inorganic materials, and ion doping, the stability of perovskites may be effectively improved. The composite structures are expected to expand the nonlinear optical applications of 2D perovskites.

5.7 Space applications

Mankind invented various spacecrafts to explore outer space, such as the International Space Station (ISS) and the Tianwen-1 Mars Probe. However, the harsh space environment featuring ultra-high vacuum, extreme temperature and containment of high-energy charged particles and rays[174] puts a high demand on equipment. Spacecraft mainly use space solar cells for energy supply. In theory, perovskite solar cells are particularly suitable for use in space due to their high PCE of above 29.1%,[184] high specific power due to sub-micron-thick absorber, low-temperature solution processability and radiation resistance. However, the study of perovskite solar cells for space applications is still in its infancy. The first report proposing this concept dates back to 2015 by Hirose and colleagues.[185] In their work, the resistance of perovskite solar cells to electron irradiation was investigated, where a 1 MeV electron irradiation source was used with a dose of 1×10^{16} particle cm^{-2} (p cm^{-2}). Using quartz as the substrate material, the performance of the device, such as short-circuit current (J_{SC}), open circuit voltage (V_{OC}) and EQE, did not decrease under electron radiation. Since then, numerous experiments have been carried out to examine the tolerance of PSC to various space irradiation, such as electron,[186] proton,[187,188] and γ-ray irradiations,[189,190] and neutrons.[191] Yan *et al.*[186] reported the excellent tolerance of perovskite solar cells under electron irradiation. After high-fluence electron irradiation of 10^{15} e cm^{-2}, the cells maintained high remaining factors of $>87.7\%$ in V_{OC} and $>93.5\%$ in the fill factor (FF) (Fig. 12a). However, the J_{SC} drastically decreased as the transmittance of substrate decreased and perovskite absorber layers decomposed partially. Neitzert *et al.*[188] fabricated an inverted perovskite solar cell in a glass/ITO/PEDOT:PSS/$CH_3NH_3PbI_3$/PCBM/BCP/Ag layer sequence with a stable PCE of 12.1% (Fig. 12b). The device was irradiated with 68 MeV protons until the total dose of 1.02×10^{13} p cm^{-2} was reached. The solar cells did not show any degradation at the proton dose of $\leq 2 \times 10^{11}$ p cm^{-2}. At the proton dose of 10^{12} and 10^{13} p cm^{-2}, the J_{SC} decreased by 10% and 40%, respectively. Therefore, the perovskite-type absorber withstood proton doses of up to 10^{12} p cm^{-2}, nearly 3 orders of magnitude higher than the damage threshold of c-Si. Moreover, the self-healing process of perovskite began and J_{SC} recovered once the proton irradiation ended. The fact that the $CH_3NH_3PbI_3$ perovskite showed both radiation resistance and self-repair ability make this type of solar cell very attractive in space applications.

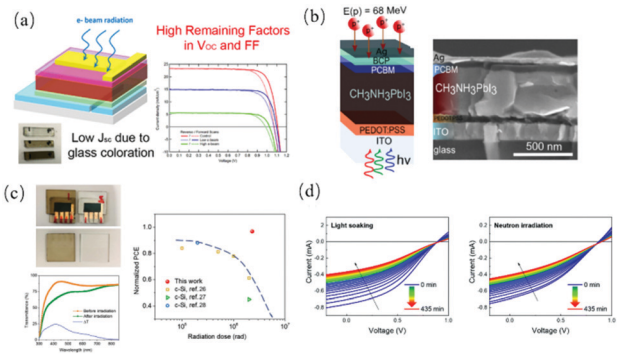

Fig. 12 (a) Schematic illustration of the perovskite solar cell and *J*–*V* curve. Adapted with permission from ref. 186. (b) Sketch of the perovskite solar cell and cross-sectional scanning electron microscopy image. Adapted with permission from ref. 188. (c) Transmission spectra of the device and ITO glass after gamma-ray irradiation, and comparison of the normalized PCE as a function of gamma-ray radiation dose for perovskite and crystal silicon solar cells. Adapted with permission from ref. 189. (d) *I*–*V* characteristics under light-soaking and neutron irradiation. Adapted with permission from ref. 191.

Huang *et al.*[189] irradiated perovskite solar cells under continuous light and gamma rays (cumulative dose of 2.3 Mrad) for 1535 h and found that they maintained excellent stability compared with glass or crystal silicon (Fig. 12c). The self-healing behavior accounted for the gamma-ray irradiation resistance given that the defect density characterization indicated that the irradiation did not impose electronic trap states. In addition, neutrons are also a type of radiation that affects aircraft. The International Space Station receives about $\approx 2.8 \times 10^{11}$ neutrons cm^{-2} per year. Cassiali *et al.*[191] reported a study on fast neutron irradiation on perovskite solar cells and found that the equipment was resilient to the dangerous radiation in space. Fast neutrons can permanently deteriorate the device performance due to the atomic displacement damage. However, the formation of neutron-induced shallow traps may work as dopants to increase the open-circuit voltage and decrease the leakage current to reduce the radiation damage on the device (Fig. 12d).

Another type of ray in space is X-rays,[192] which are electromagnetic radiation with a very short wavelength between ultraviolet and gamma rays. Metal halide perovskites of $MAPbBr_3$ were applied as semiconductor-based X-ray detectors.[193] 3D perovskite $CsPbBr_3$ nanocrystals[194] and nanosheets[195] have been reported as scintillator screens in X-ray imaging.[196] However, their practical applications remain plagued by the instability and low density of 3D perovskite nanomaterials. Accordingly, 2D bulk perovskites may offer alternative solutions. Dang *et al.*[197] used lithium chemical doping in a 2D $(PEA)_2PbBr_4$ crystal and the scintillation mechanism was explored through temperature-dependent X-ray and thermoluminescence measurements. The crystal demonstrated a fast decay time of 11 ns (80%), a sharp

peak with 12.4% energy resolution, and a scintillation yield of 11 000 photons per MeV under 662 keV gamma radiation.

It should be noted that perovskite-based nonlinear optical devices (optical limiters and saturable absorbers for mode-locking) may also find applications in space lasers and laser protection, but their study remains scant.[174]

6. Perspectives

Herein, we reviewed the latest development on 2D perovskite composites and their versatile applications. Although great progress has been made in the past few years, the research based on 2D perovskite composite structures is still in its infancy. Future studies should focus on the following issues.

AI-assisted functionalization of 2D halide perovskites

To fully realize the potential 2D perovskite composites and achieve the "1 + 1 > 2" effect, further methodologies of functionalization of 2D perovskites are necessary. 2D halide perovskites provide a good platform for defect regulation and surface functionalization given that most of their atoms are exposed to the external environment. In addition, because of their ultra-smooth surface and strong interface coupling, composite structures of ultra-thin 2D perovskites can be designed flexibly without considering the lattice mismatch.[198] Alternatively, the long-term stability of 2D perovskites is still a great challenge. Currently, the following strategies are mostly employed: (1) rationally selecting polymers with specific functional groups and anchoring them on the perovskite surface, thus preventing the perovskites from damage caused by light, high temperature, moisture and other polar solvents and (2) directly stacking perovskites with graphene, h-BN, TMDs and other 2D materials.

In this context, artificial intelligence (AI)-assisted functionalization has proven to be very effective for the rational design of 2D perovskite composites and is the future trend. The trial-and-error method based on artificial experience has become a powerful method to design new materials. At present, there are more than 40 000 papers on chemical materials assisted by machine learning.[199,200] Generally, organic cationic structures can be artificially designed and compounded with functional materials to improve the performance of 2D perovskites. Identifying the key units conducive to high performance and establishing the relationship between substructure and performance is very important for the development of new materials. However, AI alone cannot meet this challenge, and thus constant and collective efforts from both theorists and experimentalists are needed.[201]

Combination of new characterization techniques and theoretical calculations for deep understanding of the new physics of perovskites

Understanding the interaction between perovskites and functional materials (such as polymers) within composites is crucial for the development of new hybrid structures. For instance, questions such as which functional groups of the polymer passivate the trap state of 2D perovskites and how the polymer affects the termination and surface energy of perovskites are frequently met in research. In addition, it is necessary to clarify how the chain packing and composition of polymers affect the diffusion of water and oxygen, as well as the overall contribution of polymers to the electronic band structure and stability. Thus, to tackle these issues, surface analysis techniques including vibrational spectroscopy, XPS, small-angle neutron scattering techniques and NMR are very effective tools. Meanwhile, time-resolved spectroscopy is the key technique for investigating excited-state dynamics and identifying the correlation between the structural and optoelectronic properties of perovskite composites, while space-resolved techniques can detect the properties of different parts of materials. The combination of time and space resolution enables the study of dynamic processes in different positions in materials. For instance, 4D ultrafast electron microscopy (4D TEM) may directly visualize perovskites and realize simultaneous atomic spatial resolution (angstrom) and femtosecond time resolution.[202,203] In summary, multi-dimensional, cross-scale, high-resolution and *in situ* characterization techniques are urgently needed for the observation of perovskite composites.

Alternatively, computation/simulation technology is very effective to promote the understanding of the interaction of composites and the development of nanometer composites with reinforced properties. For example, DFT and molecular dynamics are expected to play increasingly important roles in investigating exciton behaviours, carrier dynamics, surface defects, interactions between surface and functional molecules of perovskites, *etc.*

Perovskite-based miniaturized and flexible devices for future IT

With the rise of new information technologies such as artificial intelligence and the Internet of Things, information processing has shifted from computing-intensive to data-intensive. Low-latency and low-energy edge computing systems are urgently needed to meet the needs of terminal devices for massive unstructured data processing capabilities in the future. For instance, biologically inspired impulsive neural networks (SNN) use sparse and asynchronous pulse sequences as input/output and process information *via* in-memory computing, which has the characteristics of large-scale parallelism and low energy consumption. Thus, to fully utilize the advantages of SNN, new synaptic electronic devices with compact and low power consumption need to be developed in hardware. Recently, biomimetic artificial synapses have made great progress, in which the two-port memristor has the advantages of simple structure and good integration, and thus regarded as an ideal carrier of bionic synapses.[204] The counterion of halide perovskite is movable under an electric field, which makes it very promising in the memristor field. Based on the excellent light absorption capacity of perovskites, these memristors can also provide novel functions through the collaborative coupling of photon, electron and ion processes. 3D halide perovskites (MA^+, FA^+ and Cs^+ as the main monovalent cations) were the

earliest and most commonly used in memristors,[205] but their stability and durability are limiting parameters. The use of 2D perovskites and their composites have recently emerged[80] but these materials have been proven to have great potential in low-cost and flexible memristors.

Ever-lasting expansion of applications

Similar to an ''all-around'' potent material, the application fields of 2D perovskite composites keep expanding. Photocatalysis such as photocatalytic CO_2 reduction[206] and water decomposition[207] is one new field they have exceled in. Composites based on perovskite nanocrystals and low-dimensional materials (such as BP,[208] graphene oxide, and MXenes) demonstrated efficacy as photocatalytic catalysts. Our group has recently combined $CsPbBr_3$ quantum dots and a 2D copper-based porphyrin MOF to construct 0D/2D hybrid catalysts for the highly efficient photocatalytic reduction of CO_2. Currently most of the reported perovskites are inorganic $CsPbBr_3$ perovskites, whereas layered 2D perovskites are much less reported.[25] However, the latter, with relatively higher stability and enhanced carrier separation efficiency[209] by introducing organic compounds, is considered more promising for photocatalysis. Moreover, controlling the growth of 2D perovskites and reducing the distance between inorganic layers may also help to improve the vertical charge transfer.

The unique bonding structure of 2D composites implies new physics and applications. Chiral 2D perovskites can be obtained by introducing chiral organic ligands into the framework. Our group reported the first example of 2D hybrid perovskite chiral ferromagnets of $(R\text{-MPEA})_2CuCl_4$ and $(S\text{-MPEA})_2CuCl_4$ (MPEA = methylphenethylamine), which showed strong oppositely signed circular dichroism signals and ferromagnetic behaviors.[210] The carriers in chiral 2D perovskites are self-polarized, and hence constructing chiral 2D perovskite composites with functional materials such as monolayer TMD can control valley polarization, providing a promising platform for spintronics. However, the spin injection process and related physical processes are unclear, which is an interesting but not widely studied field.[211]

Due to the rich structural diversity and ''soft crystal'' nature of 2D perovskites, magnetism and thermochromism can be integrated through the chemical adjustment of their organic spacer cations and metal ions,[212] which offers the possibility of using these composites not only in optoelectronic devices but also in sensing applications such as monitoring of dopamine,[213] CBr_4,[214] temperature,[215] *etc.* In addition, doping rare earth elements can realize the potential of 2D perovskites as light/heat switchable markers and high-efficiency thermometers in biomedical imaging and diagnosis. The record photoluminescence and electroluminescence efficiency[216] of 2D perovskites has continuously been broken in displays, encryption, biological imaging and X-ray detection.[52,217,218] For instance, Chandra *et al.*[219] reported the use of specific antibody-attached water-resistant $CsPbBr_3$ nanocrystals in different dimensions for two-photon imaging of breast cancer cells in the near IR region, which is superior to conventional organic fluorescence labels.

Finally, scaling-up (such as large-scale continuous) production is critical for 2D perovskite composites to move closer to commercial applications.[220] In summary, 2D halide perovskite composites have shown great potential and researchers have made continuous progress in terms of their synthesis, fundamental understanding of composition–structure–property relationships, and various applications beyond optoelectronic use. We provided our insights into the future trend of this exciting field, which will hopefully promote joint efforts from research groups of different backgrounds to tackle the current challenges.

Conflicts of interest

There are no conflicts to declare.

Acknowledgements

This work is supported by the National Natural Science Foundation of China (NSFC 22073038, 51525303, 21233001), Key Research and Development Program of Gansu Province (20YF3WA013), Open Fund of National Key Laboratory of Materials Behavior and Evaluation Technology in Space Environment (6142910200106) and Supercomputing Center of Lanzhou University.

Notes and references

1 C. Zhou, Y. Tian, M. Wang, A. Rose, T. Besara, N. K. Doyle, Z. Yuan, J. C. Wang, R. Clark, Y. Hu, T. Siegrist, S. Lin and B. Ma, *Angew. Chem., Int. Ed.*, 2017, **56**, 9018–9022.
2 G. H. Ahmed, J. Yin, R. Bose, L. Sinatra, E. Alarousu, E. Yengel, N. M. AlYami, M. I. Saidaminov, Y. Zhang, M. N. Hedhili, O. M. Bakr, J.-L. Brédas and O. F. Mohammed, *Chem. Mater.*, 2017, **29**, 4393–4400.
3 J. Qian, Q. Guo, L. Liu, B. Xu and W. Tian, *J. Mater. Chem. A*, 2017, **5**, 16786–16795.
4 J. A. Sichert, Y. Tong, N. Mutz, M. Vollmer, S. Fischer, K. Z. Milowska, R. García Cortadella, B. Nickel, C. Cardenas-Daw, J. K. Stolarczyk, A. S. Urban and J. Feldmann, *Nano Lett.*, 2015, **15**, 6521–6527.
5 Y. Bekenstein, B. A. Koscher, S. W. Eaton, P. Yang and A. P. Alivisatos, *J. Am. Chem. Soc.*, 2015, **137**, 16008–16011.
6 B. Vargas, E. Ramos, E. Pérez-Gutiérrez, J. C. Alonso and D. Solis-Ibarra, *J. Am. Chem. Soc.*, 2017, **139**, 9116–9119.
7 C. M. M. Soe, C. C. Stoumpos, M. Kepenekian, B. Traoré, H. Tsai, W. Nie, B. Wang, C. Katan, R. Seshadri, A. D. Mohite, J. Even, T. J. Marks and M. G. Kanatzidis, *J. Am. Chem. Soc.*, 2017, **139**, 16297–16309.
8 L. Mao, W. Ke, L. Pedesseau, Y. Wu, C. Katan, J. Even, M. R. Wasielewski, C. C. Stoumpos and M. G. Kanatzidis, *J. Am. Chem. Soc.*, 2018, **140**, 3775–3783.
9 C. C. Stoumpos, D. H. Cao, D. J. Clark, J. Young, J. M. Rondinelli, J. I. Jang, J. T. Hupp and M. G. Kanatzidis, *Chem. Mater.*, 2016, **28**, 2852–2867.

10 C. C. Stoumpos, C. M. M. Soe, H. Tsai, W. Nie, J.-C. Blancon, D. H. Cao, F. Liu, B. Traoré, C. Katan, J. Even, A. D. Mohite and M. G. Kanatzidis, *Chem*, 2017, **2**, 427–440.
11 S. Sun, D. Yuan, Y. Xu, A. Wang and Z. Deng, *ACS Nano*, 2016, **10**, 3648–3657.
12 L. Mao, C. C. Stoumpos and M. G. Kanatzidis, *J. Am. Chem. Soc.*, 2019, **141**, 1171–1190.
13 Z. Gan, Y. Cheng, W. Chen, K. P. Loh, B. Jia and X. Wen, *Adv. Sci.*, 2021, **8**, 2001843.
14 A. Kojima, K. Teshima, Y. Shirai and T. Miyasaka, *J. Am. Chem. Soc.*, 2009, **131**, 6050–6051.
15 M. Yuan, L. N. Quan, R. Comin, G. Walters, R. Sabatini, O. Voznyy, S. Hoogland, Y. Zhao, E. M. Beauregard, P. Kanjanaboos, Z. Lu, D. H. Kim and E. H. Sargent, *Nat. Nanotechnol.*, 2016, **11**, 872–877.
16 A. Z. Chen and J. J. Choi, *J. Vac. Sci. Technol., A*, 2020, **38**, 010801.
17 Y. Chen, Y. Sun, J. Peng, J. Tang, K. Zheng and Z. Liang, *Adv. Mater.*, 2018, **30**, 1703487.
18 X. Fu, B. Chen, J. Tang, M. T. Hassan and A. H. Zewail, *Science*, 2017, **355**, 494–498.
19 L. Qian, Y. Sun, M. Wu, C. Li, D. Xie, L. Ding and G. Shi, *Nanoscale*, 2018, **10**, 6837–6843.
20 C. Gu and J.-S. Lee, *ACS Nano*, 2016, **10**, 5413–5418.
21 K. Meng, L. Wu, Z. Liu, X. Wang, Q. Xu, Y. Hu, S. He, X. Li, T. Li and G. Chen, *Adv. Mater.*, 2018, **30**, 1706401.
22 X.-P. Zhai, B. Ma, Q. Wang and H.-L. Zhang, *Phys. Chem. Chem. Phys.*, 2020, **22**, 22140–22156.
23 H.-T. Hsu, D.-L. Yang, L. D. Wiyanto and J.-Y. Chen, *Adv. Photonics Res.*, 2021, **2**, 2000185.
24 Z. Chu, Q. Ye, Y. Zhao, F. Ma, Z. Yin, X. Zhang and J. You, *Adv. Mater.*, 2021, **33**, 2007169.
25 N. Li, X.-P. Zhai, W.-K. Yan, Y.-J. Zhang, Z.-T. Zhang, M.-J. Xiao, X.-D. Zhang, Q. Wang and H.-L. Zhang, *Sol. RRL*, 2021, **5**, 2100558.
26 W. Haizhen, M. Jiaqi and L. Dehui, *J. Phys. Chem. Lett.*, 2021, **12**, 8178–8187.
27 C. Tan, X. Cao, X.-J. Wu, Q. He, J. Yang, X. Zhang, J. Chen, W. Zhao, S. Han, G.-H. Nam, M. Sindoro and H. Zhang, *Chem. Rev.*, 2017, **117**, 6225–6331.
28 C. Chang, Y. Chen, Y.-H. Chen, Y. Chen, F. Ding, C.-H. Fan, H.-J. Fan, Z.-X. Fan, C. Gong, Y.-J. Gong, Q.-Y. He, X. Hong, S. Hu, W.-D. Hu, W. Huang, Y. Huang, W. Ji, D.-H. Li, L.-J. Li, Q. Li, L. Lin, C.-Y. Ling, M.-H. Liu, N. Liu, Z. Liu, K.-P. Loh, J.-M. Ma, F. Miao, H.-L. Peng, M.-F. Shao, L. Song, S. Su, S. Sun, C.-L. Tan, Z. D. Tang, D.-S. Wang, H. Wang, J.-L. Wang, X. Wang, X.-R. Wang, A. T. S. Wee, Z. M. Wei, Y. Wu, Z.-S. Wu, J. Xiong, Q.-H. Xiong, W.-G. Xu, P. Yin, H.-B. Zeng, Z.-Y. Zeng, T.-Y. Zhai, H. Zhang, H. Zhang, Q.-C. Zhang, T. R. Zhang, X. Zhang, L.-D. Zhao, M.-T. Zhao, W.-J. Zhao, Y.-X. Zhao, K.-G. Zhou, X. Zhou, Y. Zhou, H.-W. Zhu, H. Zhang and Z.-F. Liu, *Acta Phys. – Chim. Sin.*, 2021, **37**, 2108017.
29 F. Chen, W. Haizhen, S. Zixi, S. Hongzhi, W. Shuai, M. Jiaqi, W. Jun, L. Hongmei and L. Dehui, *ACS Appl. Mater. Interfaces*, 2019, **11**, 8419–8427.
30 E. Z. Shi, Y. Gao, B. P. Finkenauer, Akriti, A. H. Coffey and L. T. Dou, *Chem. Soc. Rev.*, 2018, **47**, 6046–6072.
31 A. G. Ricciardulli, S. Yang, J. H. Smet and M. Saliba, *Nat. Mater.*, 2021, **20**, 1325–1336.
32 J. Song, L. Xu, J. Li, J. Xue, Y. Dong, X. Li and H. Zeng, *Adv. Mater.*, 2016, **28**, 4861–4869.
33 J. Shamsi, Z. Dang, P. Bianchini, C. Canale, F. D. Stasio, R. Brescia, M. Prato and L. Manna, *J. Am. Chem. Soc.*, 2016, **138**, 7240–7243.
34 A. Pan, B. He, X. Fan, Z. Liu, J. J. Urban, A. P. Alivisatos, L. He and Y. Liu, *ACS Nano*, 2016, **10**, 7943–7954.
35 L. Dou, A. B. Wong, Y. Yu, M. Lai, N. Kornienko, S. W. Eaton, A. Fu, C. G. Bischak, J. Ma, T. Ding, N. S. Ginsberg, L.-W. Wang, A. P. Alivisatos and P. Yang, *Science*, 2015, **349**, 1518–1521.
36 S. Enzheng, Y. Biao, B. S. Stephen, G. Yao, Akriti, G. Yunfan, S. Cong, L. Minliang, Y. Peidong, K. Jing, M. S. Brett, Y. Yi and D. Letian, *Nature*, 2020, **580**, 614–620.
37 W. Deng, X. Jin, Y. Lv, X. Zhang, X. Zhang and J. Jie, *Adv. Funct. Mater.*, 2019, **29**, 1903861.
38 L. Ma, C. Wang, Y. Chu, Y. Guo, X. Feng, Z. Yu, H. Zhang and G. Zhao, *2D Mater.*, 2021, **8**, 021003.
39 M. Y. Kuo, N. Spitha, M. P. Hautzinger, P. L. Hsieh, J. Li, D. Pan, Y. Zhao, L. J. Chen, M. H. Huang, S. Jin, Y. J. Hsu and J. C. Wright, *J. Am. Chem. Soc.*, 2021, **143**, 4969–4978.
40 Y. Wang, Y. Shi, G. Xin, J. Lian and J. Shi, *Cryst. Growth Des.*, 2015, **15**, 4741–4749.
41 Y. Z. Xue, J. Yuan, J. Y. Liu and S. J. Li, *Nanomaterials*, 2018, **8**, 591–595.
42 K. Ming-Yu, S. Natalia, P. H. Matthew, H. Pei-Lun, L. Jing, P. Dongxu, Z. Yuzhou, C. Lih-Juann, H. H. Michael, J. Song, H. Yung-Jung and C. W. John, *J. Am. Chem. Soc.*, 2021, **143**, 4969–4978.
43 S. T. Ha, X. Liu, Q. Zhang, D. Giovanni, T. C. Sum and Q. Xiong, *Adv. Mater.*, 2014, **2**, 838–844.
44 Y. Chen, Y. Sun, J. Peng, J. Tang, K. Zheng and Z. Liang, *Adv. Mater.*, 2018, **30**, 1703487.
45 Z. Liu, L. Ma, G. Shi, W. Zhou, Y. Gong, S. Lei, X. Yang, J. Zhang, J. Yu, K. P. Hackenberg, A. Babakhani, J.-C. Idrobo, R. Vajtai, J. Lou and P. M. Ajayan, *Nat. Nanotechnol.*, 2013, **8**, 119–124.
46 T. Zhenjun, W. Yue, H. Hao, Y. Jianbo, Z. Jincan, L. Li, W. Mingzhan, S. Xiao, S. Luzhao, H. Yucheng, L. Kaihui, L. Zhongfan and P. Hailin, *J. Am. Chem. Soc.*, 2016, **138**, 16612–16615.
47 H.-C. Cheng, G. Wang, D. Li, Q. He, A. Yin, Y. Liu, H. Wu, M. Ding, Y. Huang and X. Duan, *Nano Lett.*, 2016, **16**, 367–373.
48 L. Junze, W. Jun, M. Jiaqi, S. Hongzhi, L. Lu, D. Xiangfeng and L. Dehui, *Nat. Commun.*, 2019, **10**, 806.
49 Y. Sun, Y. Yin, M. Pols, J. Zhong, Z. Huang, B. Liu, J. Liu, W. Wang, H. Xie, G. Zhan, Z. Zhou, W. Zhang, P. Wang, C. Zha, X. Jiang, Y. Ruan, C. Zhu, G. Brocks, X. Wang, L. Wang, J. Wang, S. Tao and W. Huang, *Adv. Mater.*, 2020, **32**, 2002392.
50 W. Qixing, Z. Qi, L. Xin, W. Junyong, Z. Rui, L. Qijie, Z. Lei, Y. Justin Zhou, W. Calvin Pei Yu, E. Goki, H. S. Jurgen and

T. S. W. Andrew, *ACS Appl. Mater. Interfaces*, 2020, **12**, 45235–45242.
51 Y.-T. Li, L. Ding, J.-Z. Li, J. Kang, D.-H. Li, L. Ren, Z.-Y. Ju, M.-X. Sun, J.-Q. Ma, Y. Tian, G.-Y. Gou, D. Xie, H. Tian, Y. Yang, L.-W. Wang, L.-M. Peng and T.-L. Ren, *ACS Cent. Sci.*, 2019, **5**, 1857–1865.
52 H. Zhang, J. Yao, Y. Yang and H. Fu, *Chem. Mater.*, 2021, **33**, 2847–2854.
53 S. Liang, M. Zhang, G. M. Biesold, W. Choi, Y. He, Z. Li, D. Shen and Z. Lin, *Adv. Mater.*, 2021, DOI: 10.1002/adma.202005888.
54 C. G.-R. María, B. F. Magnus, K. D. Rajeev, F. J. Wolter, S. Ward van der and C. G. Ferdinand, *Nat. Commun.*, 2020, **11**, 1901.
55 Z. Li, L. Kong, S. Huang and L. Li, *Angew. Chem., Int. Ed.*, 2017, **56**, 8134–8138.
56 D. N. Dirin, L. Protesescu, D. Trummer, I. V. Kochetygov, S. Yakunin, F. Krumeich, N. P. Stadie and M. V. Kovalenko, *Nano Lett.*, 2016, **16**, 5866–5874.
57 Y. He, Y. Liang, S. Liang, Y. W. Harn, Z. Li, M. Zhang, D. Shen, Z. Li, Y. Yan, X. Pang and Z. Lin, *Angew. Chem., Int. Ed.*, 2021, **60**, 7259–7266.
58 V. P. James, J. F. Daniel, A. S. Nicholas, P. H. Mark, S. Hiroaki, L. S. Charlotte and I. S. Samuel, *J. Am. Chem. Soc.*, 2018, **140**, 7313–7323.
59 B. Saparov and D. B. Mitzi, *Chem. Rev.*, 2016, **116**, 4558–4596.
60 T. M. V. G. Wouter, H. Roald, H. Kristof Van, R. Bart, D. H. Jan, L. Laurence and V. Dirk, *Chem. Commun.*, 2019, **55**, 2481–2484.
61 C. G.-R. María, T. M. V. G. Wouter, H. Roald, L. Laurence, V. Dirk and C. G. Ferdinand, *J. Phys. Chem. Lett.*, 2020, **11**, 824–830.
62 W. Yuanzhi, F. Guitao, M. Peng, L. Yigang, Z. Jing, C. Ningli, Y. Haixia, L. Weiwei, Y. Shiyong and W. Jizheng, *ACS Appl. Mater. Interfaces*, 2020, **12**, 8826–8834.
63 X. Gong, O. Voznyy, A. Jain, W. Liu, R. Sabatini, Z. Piontkowski, G. Walters, G. Bappi, S. Nokhrin, O. Bushuyev, M. Yuan, R. Comin, D. McCamant, S. O. Kelley and E. H. Sargent, *Nat. Mater.*, 2018, **17**, 550–556.
64 Y.-H. Kim, S. Kim, A. Kakekhani, J. Park, J. Park, Y.-H. Lee, H. Xu, S. Nagane, R. B. Wexler, D.-H. Kim, S. H. Jo, L. Martínez-Sarti, P. Tan, A. Sadhanala, G.-S. Park, Y.-W. Kim, B. Hu, H. J. Bolink, S. Yoo, R. H. Friend, A. M. Rappe and T.-W. Lee, *Nat. Photonics*, 2021, **15**, 148–155.
65 M. Saliba, J.-P. Correa-Baena, M. Grätzel, A. Hagfeldt and A. Abate, *Angew. Chem., Int. Ed.*, 2018, **57**, 2554–2569.
66 S. De Wolf, J. Holovsky, S.-J. Moon, P. Löper, B. Niesen, M. Ledinsky, F.-J. Haug, J.-H. Yum and C. Ballif, *J. Phys. Chem. Lett.*, 2014, **5**, 1035–1039.
67 C. Huo, B. Cai, Z. Yuan, B. Ma and H. Zeng, *Small Methods*, 2017, **1**, 1600018.
68 Z. Tan, Y. Wu, H. Hong, J. Yin, J. Zhang, L. Lin, M. Wang, X. Sun, L. Sun, Y. Huang, K. Liu, Z. Liu and H. Peng, *J. Am. Chem. Soc.*, 2016, **138**, 16612–16615.
69 N. N. Wang, L. Cheng, R. Ge, S. T. Zhang, Y. F. Miao, W. Zou, C. Yi, Y. Sun, Y. Cao, R. Yang, Y. Q. Wei, Q. Guo, Y. Ke, M. T. Yu, Y. Z. Jin, Y. Liu, Q. Q. Ding, D. W. Di, L. Yang, G. C. Xing, H. Tian, C. H. Jin, F. Gao, R. H. Friend, J. P. Wang and W. Huang, *Nat. Photonics*, 2016, **10**, 699–704.
70 L. N. Quan, Y. Zhao, F. P. Garcia de Arquer, R. Sabatini, G. Walters, O. Voznyy, R. Comin, Y. Li, J. Z. Fan, H. Tan, J. Pan, M. Yuan, O. M. Bakr, Z. Lu, D. H. Kim and E. H. Sargent, *Nano Lett.*, 2017, **17**, 3701–3709.
71 J. Xing, Y. B. Zhao, M. Askerka, L. N. Quan, X. W. Gong, W. J. Zhao, J. X. Zhao, H. R. Tan, G. K. Long, L. Gao, Z. Y. Yang, O. Voznyy, J. Tang, Z. H. Lu, Q. H. Xiong and E. H. Sargent, *Nat. Commun.*, 2018, **9**, 3541.
72 M. Ahmadi, T. Wu and B. Hu, *Adv. Mater.*, 2017, **29**, 1605242.
73 M. D. Smith, L. Pedesseau, M. Kepenekian, I. C. Smith, C. Katan, J. Even and H. I. Karunadasa, *Chem. Sci.*, 2017, **8**, 1960–1968.
74 J. C. Blancon, J. Even, C. C. Stoumpos, M. G. Kanatzidis and A. D. Mohite, *Nat. Nanotechnol.*, 2020, **15**, 969–985.
75 H. L. Wang, W. Z. Lv, X. X. Tang, L. F. Chen, R. F. Chen and W. Huang, *Prog. Chem.*, 2017, **29**, 859–869.
76 X. Qi, Y. Zhang, Q. Ou, S. T. Ha, C.-W. Qiu, H. Zhang, Y.-B. Cheng, Q. Xiong and Q. Bao, *Small*, 2018, **14**, 1800682.
77 H. Peiman, C. D. Wright and B. Harish, *Nature*, 2014, **511**, 206–211.
78 X. Zhao, H. Xu, Z. Wang, Y. Lin and Y. Liu, *InfoMat*, 2019, **1**, 183–210.
79 Z. Xiao and J. Huang, *Adv. Electron. Mater.*, 2016, **2**, 1600100.
80 H. Tian, L. Zhao, X. Wang, Y.-W. Yeh, N. Yao, B. P. Rand and T.-L. Ren, *ACS Nano*, 2017, **11**, 12247–12256.
81 W. R. Mateker and M. D. McGehee, *Adv. Mater.*, 2017, **29**, 1603940.
82 B.-X. Du, Z.-J. Quan, Y.-X. Da, Z. Zhang and X.-C. Wang, *Adv. Synth. Catal.*, 2015, **357**, 1270–1276.
83 Y. Lin, Y. Bai, Y. Fang, Q. Wang, Y. Deng and J. Huang, *ACS Energy Lett.*, 2017, **2**, 1571–1572.
84 X. Xiao, J. Dai, Y. Fang, J. Zhao, X. Zheng, S. Tang, P. N. Rudd, X. C. Zeng and J. Huang, *ACS Energy Lett.*, 2018, **3**, 684–688.
85 G. Dresselhaus, A. F. Kip and C. Kittel, *Phys. Rev.*, 1954, **95**, 568–569.
86 Y. Zhai, S. Baniya, C. Zhang, J. Li, P. Haney, C.-X. Sheng, E. Ehrenfreund and V. Vardeny Zeev, *Sci. Adv.*, 2017, **3**, 1700704.
87 J. Yin, P. Maity, L. Xu, A. M. El-Zohry, H. Li, O. M. Bakr, J.-L. Brédas and O. F. Mohammed, *Chem. Mater.*, 2018, **30**, 8538–8545.
88 Y. Jun, N. Rounak, M. Partha, G.-A. Luis, A. Dhaifallah, S. R. Iman, B. Jean-Luc, M. B. Osman and F. M. Omar, *Nat. Commun.*, 2021, **12**, 3995.
89 N. Li, Q. Wang and H.-L. Zhang, *Chem. Rec.*, 2020, **20**, 413–428.
90 X. Zhai, Y. Huang, Z. Feng, X. Zhang and Q. Wang, in *Quantum Dot Optoelectronic Devices*, ed. P. Yu and

Z. M. Wang, Springer International Publishing, Cham, 2020, DOI: 10.1007/978-3-030-35813-6_6.
91 V. A. Hintermayr, L. Polavarapu, A. S. Urban and J. Feldmann, *ACS Nano*, 2018, **12**, 10151–10158.
92 Z.-P. Huang, B. Ma, H. Wang, N. Li, R.-T. Liu, Z.-Q. Zhang, X.-D. Zhang, J.-H. Zhao, P.-Z. Zheng, Q. Wang and H.-L. Zhang, *J. Phys. Chem. Lett.*, 2020, **11**, 6007–6015.
93 A. Brumberg, B. T. Diroll, G. Nedelcu, M. E. Sykes, Y. Liu, S. M. Harvey, M. R. Wasielewski, M. V. Kovalenko and R. D. Schaller, *Nano Lett.*, 2018, **18**, 4771–4776.
94 G. Ghosh, A. Dutta, A. Ghosh, S. Ghosh and A. Patra, *J. Phys. Chem. C*, 2020, **124**, 10252–10260.
95 Y. Yang, D. P. Ostrowski, R. M. France, K. Zhu, J. van de Lagemaat, J. M. Luther and M. C. Beard, *Nat. Photonics*, 2015, **10**, 53–59.
96 J. Fu, Q. Xu, G. Han, B. Wu, C. H. A. Huan, M. L. Leek and T. C. Sum, *Nat. Commun.*, 2017, **8**, 1300.
97 Z.-Y. Zhu, Q.-Q. Yang, L.-F. Gao, L. Zhang, A.-Y. Shi, C.-L. Sun, Q. Wang and H.-L. Zhang, *J. Phys. Chem. Lett.*, 2017, **8**, 1610–1614.
98 Y. Li, W. Zhou, Y. Li, W. Huang, Z. Zhang, G. Chen, H. Wang, G.-H. Wu, N. Rolston, R. Vila, W. Chiu and Y. Cui, *Joule*, 2019, **3**, 2854–2866.
99 D. W. deQuilettes, W. Zhang, V. M. Burlakov, D. J. Graham, T. Leijtens, A. Osherov, V. Bulović, H. J. Snaith, D. S. Ginger and S. D. Stranks, *Nat. Commun.*, 2016, **7**, 11683–11692.
100 Y. Lu, J. Hu, Y. Ge, B. Tian, Z. Zhang and M. Sui, *J. Mater. Chem. A*, 2021, **9**, 15059–15067.
101 L. Piveteau, V. Morad and M. V. Kovalenko, *J. Am. Chem. Soc.*, 2020, **142**, 19413–19437.
102 J. Lee, W. Lee, K. Kang, T. Lee and S. K. Lee, *Chem. Mater.*, 2020, **33**, 370–377.
103 B. A. Rosales, L. Men, S. D. Cady, M. P. Hanrahan, A. J. Rossini and J. Vela, *Chem. Mater.*, 2016, **28**, 6848–6859.
104 Z. Fan, H. Xiao, Y. L. Wang, Z. P. Zhao, Z. Y. Lin, H. C. Cheng, S. J. Lee, G. M. Wang, Z. Y. Feng, W. A. Goddard, Y. Huang and X. F. Duan, *Joule*, 2017, **1**, 548–562.
105 L. Piveteau, V. Morad and M. V. Kovalenko, *J. Am. Chem. Soc.*, 2020, **142**, 19413–19437.
106 J.-C. Blancon, H. Tsai, W. Nie, C. C. Stoumpos, L. Pedesseau, C. Katan, M. Kepenekian, C. M. M. Soe, K. Appavoo, M. Y. Sfeir, S. Tretiak, P. M. Ajayan, M. G. Kanatzidis, J. Even, J. J. Crochet and A. D. Mohite, *Science*, 2017, **355**, 1288–1292.
107 X. Jiang, J. Hoffman, C. C. Stoumpos, M. G. Kanatzidis and E. Harel, *ACS Energy Lett.*, 2019, **4**, 1741–1747.
108 O. F. Williams, N. Zhou, J. Hu, Z. Ouyang, A. Kumbhar, W. You and A. M. Moran, *J. Phys. Chem. A*, 2019, **123**, 11012–11021.
109 C. Zhao, W. Tian, J. Leng, Y. Zhao and S. Jin, *J. Phys. Chem. Lett.*, 2019, **10**, 3950–3954.
110 C. Zhao, W. Tian, Q. Sun, Z. Yin, J. Leng, S. Wang, J. Liu, K. Wu and S. Jin, *J. Am. Chem. Soc.*, 2020, **142**, 15091–15097.
111 G. Divitini, S. Cacovich, F. Matteocci, L. Cinà, A. D. Carlo and C. Ducati, *Nat. Energy*, 2016, **1**, 15012.
112 L. Wei-Chun, L. Wei-Chun, L. Jun-Xian, W. Yi-Kai, T. Jui-Fu and F. Zi-Yun, *npj Mater. Degrad.*, 2021, **5**, 13.
113 M. Keisuke, M. Yu, K. Daisuke, I. Masashi, M. Tsutomu, Y. Tomoyuki and H. Kazuyuki, *J. Appl. Phys.*, 2017, **121**, 085501.
114 H. J. Jung, D. Kim, S. Kim, J. Park, V. P. Dravid and B. Shin, *Adv. Mater.*, 2018, **30**, 1802769.
115 J. S. Yoo, G. S. Han, S. Lee, M. C. Kim, M. Choi, H. S. Jung and J.-K. Lee, *Nano Res.*, 2017, **10**, 3885–3895.
116 D. G. Lee, M.-c. Kim, S. Wang, B. J. Kim, Y. S. Meng and H. S. Jung, *ACS Appl. Mater. Interfaces*, 2019, **11**, 48497–48504.
117 C. Lan, Z. Zhou, R. Wei and J. C. Ho, *Mater. Today Energy*, 2019, **11**, 61–82.
118 F. Zhang, H. Lu, J. Tong, J. J. Berry, M. C. Beard and K. Zhu, *Energy Environ. Sci.*, 2020, **13**, 1154–1186.
119 Z. K. Tan, R. S. Moghaddam, M. L. Lai, P. Docampo, R. Higler, F. Deschler, M. Price, A. Sadhanala, L. M. Pazos, D. Credgington, F. Hanusch, T. Bein, H. J. Snaith and R. H. Friend, *Nat. Nanotechnol.*, 2014, **9**, 687–692.
120 Z. Chu, Q. Ye, Y. Zhao, F. Ma, Z. Yin, X. Zhang and J. You, *Adv. Mater.*, 2021, **33**, 2007169.
121 S. Chen and G. Q. Shi, *Adv. Mater.*, 2017, **29**, 1605448.
122 B. Zhao, S. Bai, V. Kim, R. Lamboll, R. Shivanna, F. Auras, J. M. Richter, L. Yang, L. Dai, M. Alsari, X.-J. She, L. Liang, J. Zhang, S. Lilliu, P. Gao, H. J. Snaith, J. Wang, N. C. Greenham, R. H. Friend and D. Di, *Nat. Photonics*, 2018, **12**, 783–789.
123 C. Sun, Y. Jiang, M. Cui, L. Qiao, J. Wei, Y. Huang, L. Zhang, T. He, S. Li, H.-Y. Hsu, C. Qin, R. Long and M. Yuan, *Nat. Commun.*, 2021, **12**, 2207.
124 Y. Ling, Z. Yuan, Y. Tian, X. Wang, J. C. Wang, Y. Xin, K. Hanson, B. Ma and H. Gao, *Adv. Mater.*, 2016, **28**, 305–316.
125 Z. Liu, W. Qiu, X. Peng, G. Sun, X. Liu, D. Liu, Z. Li, F. He, C. Shen, Q. Gu, F. Ma, H.-L. Yip, L. Hou, Z. Qi and S.-J. Su, *Adv. Mater.*, 2021, **33**, 2103268.
126 X. Xu, H. He, J. Li, Z. Fang, L. Gan, L. Chen and Z. Ye, *ACS Appl. Mater. Interfaces*, 2019, **11**, 8436–8442.
127 J. Y. Jason, S. Gabkyung, R. C. Matthew, P. Tae Gwan, L. Yongli, R. Fabian, K. Young-Ki, M. Chan Su, J. Nam Joong, C.-B. Juan-Pablo, B. Vladimir, S. Seong Sik, G. B. Moungi and S. Jangwon, *Nature*, 2021, **590**, 587–593.
128 H. C. Duyen, C. S. Constantinos, K. F. Omar, T. H. Joseph and G. K. Mercouri, *J. Am. Chem. Soc.*, 2015, **137**, 7843–7850.
129 P. Li, Y. Zhang, C. Liang, G. Xing, X. Liu, F. Li, X. Liu, X. Hu, G. Shao and Y. Song, *Adv. Mater.*, 2018, **30**, 1805323.
130 L. Chao, G. Hao, X. Yingdong, W. Zhuo, L. Xiaotao, X. Junmin, Z. Shouwei, H. Yue, G. Xingyu, H. Wei, C. Lingfeng, N. Tingting, F. Min, L. Hui, D. Han, Y. Hui, C. Shi, R. Xueqin, S. Lin, L. Bixin, Z. Jing, P. Yong, S. Guosheng, W. Jianpu, C. Yonghua, X. Guichuan and H. Wei, *Nat. Energy*, 2020, **6**, 38–45.
131 W. Zhiping, L. Qianqian, P. C. Francis, S. Nobuya, M. H. Laura and J. S. Henry, *Nat. Energy*, 2017, **2**, 17135.

132 G. Liu, H. Zheng, X. Xu, S. Xu, X. Zhang, X. Pan and S. Dai, *Adv. Funct. Mater.*, 2019, **29**, 1807565.
133 Z. Yang, W. Zeyang, H. Shu, Y. Pingyuan, L. Heng and S. ChuanXiang, *ACS Appl. Mater. Interfaces*, 2021, **13**, 12042–12048.
134 J. Yeoun-Woo, L. Seungmin, Y. Kyung Mun, J. Kiwan, C. Kwang, C. Mansoo and N. Jun Hong, *Nat. Energy*, 2021, **6**, 63–71.
135 Q. Zhang, Q. Shang, R. Su, T. T. H. Do and Q. Xiong, *Nano Lett.*, 2021, **21**, 1903–1914.
136 Q. Zhang, S. T. Ha, X. Liu, T. C. Sum and Q. Xiong, *Nano Lett.*, 2014, **14**, 5995–6001.
137 H. Zhang, Q. Liao, Y. Wu, Z. Zhang, Q. Gao, P. Liu, M. Li, J. Yao and H. Fu, *Adv. Mater.*, 2018, **30**, 1706186.
138 S. Q. Li, D. Y. Lei, W. Ren, X. Y. Guo, S. F. Wu, Y. Zhu, A. L. Rogach, M. Chhowalla and A. K. Y. Jen, *Nat. Commun.*, 2020, **11**, 1192.
139 A. A. Balandin, *Nat. Mater.*, 2011, **10**, 569–581.
140 M. J. Meziani, W. L. Song, P. Wang, F. Lu, Z. Hou, A. Anderson, H. Maimaiti and Y. P. Sun, *Chem. Phys. Chem.*, 2015, **16**, 1339–1346.
141 Z. Fan, H. Xiao, Y. Wang, Z. Zhao, Z. Lin, H.-C. Cheng, S.-J. Lee, G. Wang, Z. Feng, W. A. Goddard, Y. Huang and X. Duan, *Joule*, 2017, **1**, 548–562.
142 H. Yu, X. Cheng, Y. Wang, Y. Liu, K. Rong, Z. Li, Y. Wan, W. Gong, K. Watanabe, T. Taniguchi, S. Wang, J. Chen, Y. Ye and L. Dai, *ACS Photonics*, 2018, **5**, 4520–4528.
143 H. Yu, X. Xu, H. Liu, Y. Wan, X. Cheng, J. Chen, Y. Ye and L. Dai, *ACS Nano*, 2020, **14**, 552–558.
144 J. Chen, P. Chábera, T. Pascher, M. E. Messing, R. Schaller, S. Canton, K. Zheng and T. Pullerits, *J. Phys. Chem. Lett.*, 2017, **8**, 5119–5124.
145 J. Li, S. Zhang, H. Dong, X. Yuan, X. Jiang, J. Wang and L. Zhang, *CrystEngComm*, 2016, **18**, 7945–7949.
146 W. Zhang, L. Peng, J. Liu, A. Tang, J.-S. Hu, J. Yao and Y. S. Zhao, *Adv. Mater.*, 2016, **28**, 4040–4046.
147 L. Li, X. Shang, S. Wang, N. Dong, C. Ji, X. Chen, S. Zhao, J. Wang, Z. Sun, M. Hong and J. Luo, *J. Am. Chem. Soc.*, 2018, **140**, 6806–6809.
148 Y. T. Li, L. Ding, J. Z. Li, J. Kang, D. H. Li, L. Ren, Z. Y. Ju, M. X. Sun, J. Q. Ma, Y. Tian, G. Y. Gou, D. Xie, H. Tian, Y. Yang, L. W. Wang, L. M. Peng and T. L. Ren, *ACS Cent. Sci.*, 2019, **5**, 1857–1865.
149 E. Ercan, J. Y. Chen, C. C. Shih, C. C. Chueh and W. C. Chen, *Nanoscale*, 2018, **10**, 18869–18877.
150 T. Leydecker, M. Herder, E. Pavlica, G. Bratina, S. Hecht, E. Orgiu and P. Samori, *Nat. Nanotechnol.*, 2016, **11**, 769–775.
151 M. Y. Liao, Y. C. Chiang, C. H. Chen, W. C. Chen and C. C. Chueh, *ACS Appl. Mater. Interfaces*, 2020, **12**, 36398–36408.
152 J. Wang, J. Li, Q. Tan, L. Li, J. Zhang, J. Zang, P. Tan, J. Zhang and D. Li, *J. Phys. Chem. Lett.*, 2017, **8**, 6211–6219.
153 J. Wang, J. Li, S. Lan, C. Fang, H. Shen, Q. Xiong and D. Li, *ACS Nano*, 2019, **13**, 5473–5484.
154 E. S. Shi, B. Yuan, S. B. Shiring, Y. Gao, Akriti, Y. F. Guo, C. Su, M. L. Lai, P. D. Yang, J. Kong, B. M. Savoie, Y. Yu and L. T. Dou, *Nature*, 2020, **580**, 614–620.
155 Y. Chen, Y. Sun, J. Peng, J. Tang, K. Zheng and Z. Liang, *Adv. Mater.*, 2018, **30**, 1703487.
156 Y. Wei, G. Feng, P. Mao, Y. Luan, J. Zhuang, N. Chen, H. Yang, W. Li, S. Yang and J. Wang, *ACS Appl. Mater. Interfaces*, 2020, **12**, 8826–8834.
157 R. Dong, C. Lan, F. Li, S. Yip and J. C. Ho, *Nanoscale Horiz.*, 2019, **4**, 1342–1352.
158 M. Min, R. F. Hossain, N. Adhikari and A. B. Kaul, *ACS Appl. Mater. Interfaces*, 2020, **12**, 10809–10819.
159 X. Li, D. Yu, J. Chen, Y. Wang, F. Cao, Y. Wei, Y. Wu, L. Wang, Y. Zhu, Z. Sun, J. Ji, Y. Shen, H. Sun and H. Zeng, *ACS Nano*, 2017, **11**, 2015–2023.
160 W. Deng, H. Huang, H. Jin, W. Li, X. Chu, D. Xiong, W. Yan, F. Chun, M. Xie, C. Luo, L. Jin, C. Liu, H. Zhang, W. Deng and W. Yang, *Adv. Opt. Mater.*, 2019, **7**, 1801521.
161 Y. Shen, D. Yu, X. Wang, C. Huo, Y. Wu, Z. Zhu and H. Zeng, *Nanotechnology*, 2018, **29**, 085201.
162 A. Yang, J. C. Blancon, W. Jiang, H. Zhang, J. Wong, E. Yan, Y. R. Lin, J. Crochet, M. G. Kanatzidis, D. Jariwala, T. Low, A. D. Mohite and H. A. Atwater, *Nano Lett.*, 2019, **19**, 4852–4860.
163 L. Zhao, H. Tian, S. H. Silver, A. Kahn, T.-L. Ren and B. P. Rand, *Joule*, 2018, **2**, 2133–2144.
164 K.-G. Lim, T.-H. Han and T.-W. Lee, *Energy Environ. Sci.*, 2021, **14**, 2009–2035.
165 L. Kai, F. Wei, L. Yanpeng, C. Manish and L. Kian Ping, *Nat. Rev. Mater.*, 2020, **5**, 482–500.
166 P. A. Franken, A. E. Hill, C. W. Peters and G. Weinreich, *Phy. Rev. Lett.*, 1961, **7**, 118–119.
167 S. Weili, C. Jun, W. Jinqiang, L. Xiaoming and Z. Haibo, *ACS Photonics*, 2020, **8**, 113–124.
168 X. Zheng, B. Jia, X. Chen and M. Gu, *Adv. Mater.*, 2014, **26**, 2699–2703.
169 X. Yin, Z. Ye, D. A. Chenet, Y. Ye, K. O'Brien, J. C. Hone and X. Zhang, *Science*, 2014, **344**, 488–490.
170 Y. Li, Y. Rao, K. F. Mak, Y. You, S. Wang, C. R. Dean and T. F. Heinz, *Nano Lett.*, 2013, **13**, 3329–3333.
171 T. Yang, I. Abdelwahab, H. Lin, Y. Bao, S. J. Rong Tan, S. Fraser, K. P. Loh and B. Jia, *ACS Photonics*, 2018, **5**, 4969–4977.
172 Q.-Q. Yang, R.-T. Liu, C. Huang, Y.-F. Huang, L.-F. Gao, B. Sun, Z.-P. Huang, L. Zhang, C.-X. Hu, Z.-Q. Zhang, C.-L. Sun, Q. Wang, Y.-L. Tang and H.-L. Zhang, *Nanoscale*, 2018, **10**, 21106–21115.
173 N. Li, Q. Wang and H.-L. Zhang, *Chem. Rec.*, 2020, **20**, 413–428.
174 Z.-T. Zhang, Q.-Q. Yang, X.-J. Zhen, Z.-Z. Feng, X.-P. Zhai, X.-D. Zhang, Y.-F. Huang, Q. Wang and H.-L. Zhang, *ACS Appl. Mater. Interfaces*, 2021, **13**, 21626–21634.
175 I. Abdelwahab, G. Grinblat, K. Leng, Y. Li, X. Chi, A. Rusydi, S. A. Maier and K. P. Loh, *ACS Nano*, 2018, **12**, 644–650.
176 C. Yuan, X. Li, S. Semin, Y. Feng, T. Rasing and J. Xu, *Nano Lett.*, 2018, **18**, 5411–5417.

177 W.-J. Wei, X.-X. Jiang, L.-Y. Dong, W.-W. Liu, X.-B. Han, Y. Qin, K. Li, W. Li, Z.-S. Lin, X.-H. Bu and P.-X. Lu, *J. Am. Chem. Soc.*, 2019, **141**, 9134–9139.
178 X. Han, Y. Zheng, S. Chai, S. Chen and J. Xu, *Nanophotonics*, 2020, **9**, 1787–1810.
179 Y. Zhou, Y. Huang, X. Xu, Z. Fan, J. B. Khurgin and Q. Xiong, *Appl. Phys. Rev.*, 2020, **7**, 041313.
180 P. Li, Y. Chen, T. Yang, Z. Wang, H. Lin, Y. Xu, L. Li, H. Mu, B. N. Shivananju, Y. Zhang, Q. Zhang, A. Pan, S. Li, D. Tang, B. Jia, H. Zhang and Q. Bao, *ACS Appl. Mater. Interfaces*, 2017, **9**, 12759–12765.
181 S. Hong, F. Lédée, J. Park, S. Song, H. Lee, Y. S. Lee, B. Kim, D.-I. Yeom, E. Deleporte and K. Oh, *Laser Photonics Rev.*, 2018, **12**, 1800118.
182 A. Mushtaq, D. Kushavah, S. Ghosh and S. K. Pal, *Appl. Phys. Lett.*, 2019, **114**, 051902.
183 S. J. Varma, J. Cherusseri, J. Li, J. Kumar, E. Barrios and J. Thomas, *AIP Adv.*, 2020, **10**, 045130.
184 A. Al-Ashouri, E. Köhnen, B. Li, A. Magomedov, H. Hempel, P. Caprioglio, J. A. Márquez, A. B. M. Vilches, E. Kasparavicius, J. A. Smith, N. Phung, D. Menzel, M. Grischek, L. Kegelmann, D. Skroblin, C. Gollwitzer, T. Malinauskas, M. Jošt, G. Matič, B. Rech, R. Schlatmann, M. Topič, L. Korte, A. Abate, B. Stannowski, D. Neher, M. Stolterfoht, T. Unold, V. Getautis and S. Albrecht, *Science*, 2020, **370**, 1300–1309.
185 M. Yu, M. Ikegami, T. Miyasaka, T. Ohshima and K. Hirose, Evaluation of radiation tolerance of perovskite solar cell for use in space, *2015 IEEE 42nd Photovoltaic Specialist Conference (PVSC)*, 2015, pp. 1–4, DOI: 10.1109/PVSC.2015.7355859.
186 Z. Song, C. Li, C. Chen, J. McNatt, W. Yoon, D. Scheiman, P. P. Jenkins, R. J. Ellingson, M. J. Heben and Y. Yan, *J. Phys. Chem. C*, 2020, **124**, 1330–1336.
187 Y. Miyazawa, M. Ikegami, H.-W. Chen, T. Ohshima, M. Imaizumi, K. Hirose and T. Miyasaka, *iScience*, 2018, **2**, 148–155.
188 F. Lang, N. H. Nickel, J. Bundesmann, S. Seidel, A. Denker, S. Albrecht, V. V. Brus, J. Rappich, B. Rech, G. Landi and H. C. Neitzert, *Adv. Mater.*, 2016, **28**, 8726–8731.
189 S. Yang, Z. Xu, S. Xue, P. Kandlakunta, L. Cao and J. Huang, *Adv. Mater.*, 2019, **31**, 1805547.
190 K. Yang, K. Huang, X. Li, S. Zheng, P. Hou, J. Wang, H. Guo, H. Song, B. Li, H. Li, B. Liu, X. Zhong and J. Yang, *Org. Electron.*, 2019, **71**, 79–84.
191 G. M. Paternò, V. Robbiano, L. Santarelli, A. Zampetti, C. Cazzaniga, V. Garcìa Sakai and F. Cacialli, *Sustainable Energy Fuels*, 2019, **3**, 2561–2566.
192 Y. Tu, J. Wu, G. Xu, X. Yang, R. Cai, Q. Gong, R. Zhu and W. Huang, *Adv. Mater.*, 2021, **33**, 2006545.
193 H. Wei, Y. Fang, P. Mulligan, W. Chuirazzi, H.-H. Fang, C. Wang, B. R. Ecker, Y. Gao, M. A. Loi, L. Cao and J. Huang, *Nat. Photonics*, 2016, **10**, 333–339.
194 Y. Zhang, R. Sun, X. Ou, K. Fu, Q. Chen, Y. Ding, L.-J. Xu, L. Liu, Y. Han, A. V. Malko, X. Liu, H. Yang, O. M. Bakr, H. Liu and O. F. Mohammed, *ACS Nano*, 2019, **13**, 2520–2525.
195 H. Wei, D. DeSantis, W. Wei, Y. Deng, D. Guo, T. J. Savenije, L. Cao and J. Huang, *Nat. Mater.*, 2017, **16**, 826–833.
196 Y. Zhou, J. Chen, O. M. Bakr and O. F. Mohammed, *ACS Energy Lett.*, 2021, **6**, 739–768.
197 A. Xie, C. Hettiarachchi, F. Maddalena, M. E. Witkowski, M. Makowski, W. Drozdowski, A. Arramel, A. T. S. Wee, S. V. Springham, P. Q. Vuong, H. J. Kim, C. Dujardin, P. Coquet, M. D. Birowosuto and C. Dang, *Commun. Mater.*, 2020, **1**, 37.
198 B. Jean-Christophe, E. Jacky, C. S. Costas, G. K. Mercouri and D. M. Aditya, *Nat. Nanotechnol.*, 2020, **15**, 969–985.
199 R. Paul, C. E. Katherine, D. F. A. Philip, F. Casey, B. W. Malia, M. Aurelio, Z. Matthias, A. F. Sorelle, S. Joshua and J. N. Alexander, *Nature*, 2016, **533**, 73–76.
200 E. Andre, K. Brett, A. N. Roberto, K. Justin, M. S. Susan, M. B. Helen and T. Sebastian, *Nature*, 2017, **542**, 115–118.
201 G.-B. Rafael, A.-I. Jorge, D. H. Timothy, D. David, M. Dougal, A. B.-F. Martin, C. Hyun Sik, E. Markus, H. Dong-Gwang, W. Tony, M. Georgios, J. Soonok, K. Hosuk, M. Hiroshi, N. Masaki, K. Sunghan, H. Wenliang, H. Seong Ik, B. Marc, P. A. Ryan and A.-G. Alán, *Nat. Mater.*, 2016, **15**, 1120–1127.
202 X. Fu, B. Chen, J. Tang, M. T. Hassan and A. H. Zewail, *Science*, 2017, **355**, 494–498.
203 G. Cao, S. Sun, Z. Li, H. Tian, H. Yang and J. Li, *Sci. Rep.*, 2015, **5**, 8404.
204 J. Ge, Z. Ma, W. Chen, X. Cao, J. Yan, H. Fang, J. Qin, Z. Liu and S. Pan, *Nanoscale*, 2020, **12**, 13558–13566.
205 T. Chang, S.-H. Jo and W. Lu, *ACS Nano*, 2011, **5**, 7669–7676.
206 Z. Liu, H. Yang, J. Wang, Y. Yuan, K. Hills-Kimball, T. Cai, P. Wang, A. Tang and O. Chen, *Nano Lett.*, 2021, **21**, 1620–1627.
207 H. Wang, H. Zhang, J. Wang, Y. Gao, F. Fan, K. Wu, X. Zong and C. Li, *Angew. Chem., Int. Ed.*, 2021, **60**, 7376–7381.
208 X. Wang, J. He, J. Li, G. Lu, F. Dong, T. Majima and M. Zhu, *Appl. Catal., B*, 2020, **277**, 119230.
209 H. Huang, B. Pradhan, J. Hofkens, M. B. J. Roeffaers and J. A. Steele, *ACS Energy Lett.*, 2020, **5**, 1107–1123.
210 B. Sun, X.-F. Liu, X.-Y. Li, Y. Zhang, X. Shao, D. Yang and H.-L. Zhang, *Chem. Mater.*, 2020, **32**, 8914–8920.
211 H. Wang, J. Ma and D. Li, *J. Phys. Chem. Lett.*, 2021, **12**, 8178–8187.
212 B. Sun, X.-F. Liu, X.-Y. Li, Y. Cao, Z. Yan, L. Fu, N. Tang, Q. Wang, X. Shao, D. Yang and H.-L. Zhang, *Angew. Chem., Int. Ed.*, 2020, **59**, 203–208.
213 C. Xu, L. Dongyu, P. Gencai, Z. Donglei, X. Wen, Z. Jinyang, W. He, C. Cong and S. Hongwei, *Nanoscale*, 2018, **10**, 10505–10513.
214 P. Nikolaou, A. Vassilakopoulou, D. Papadatos, E. Topoglidis and I. Koutselas, *Mater. Chem. Front.*, 2018, **2**, 730–740.

215 C. Daqin, C. Xiao, L. Xiaoyue, G. Hai, L. Shen and L. Xinyue, *Opt. Lett.*, 2017, **42**, 4950.
216 C. Katan, N. Mercier and J. Even, *Chem. Rev.*, 2019, **119**, 3140–3192.
217 X.-F. Liu, L. Zou, C. Yang, W. Zhao, X.-Y. Li, B. Sun, C.-X. Hu, Y. Yu, Q. Wang, Q. Zhao and H.-L. Zhang, *ACS Appl. Mater. Interfaces*, 2020, **12**, 43073–43082.
218 J. Peng, C. Q. Xia, Y. Xu, R. Li, L. Cui, J. K. Clegg, L. M. Herz, M. B. Johnston and Q. Lin, *Nat. Commun.*, 2021, **12**, 1531.
219 A. Pramanik, S. Patibandla, Y. Gao, K. Gates and P. C. Ray, *JACS Au*, 2021, **1**, 53–65.
220 G. M. Biesold, S. Liang, B. K. Wagner, Z. Kang and Z. Lin, *Nanoscale*, 2021, **13**, 13108–13115.